



Review of Chalcogenide-Based Materials for Low-, Mid-, and High-Temperature Thermoelectric Applications

Suchitra Puthran¹ · Ganesh Shridhar Hegde² · Ashwatha Narayana Prabhu¹

Received: 22 December 2023 / Accepted: 1 July 2024 / Published online: 27 July 2024
© The Author(s) 2024

Abstract

Thermoelectric materials possess the capability to convert electricity into heat and vice versa. The utilization of chloro-fluorocarbons and hydrochlorofluorocarbons as thermal carrier agents in traditional cooling and air conditioning systems has sparked a surge in exploration toward pioneering refrigeration and spatial conditioning technologies. Chalcogenides, known for their capacity to amplify the thermoelectric efficiency of materials and their adaptability across a broad spectrum of temperatures, stand out as pivotal components in thermoelectric materials. Despite their existing suboptimal performance, these materials hold substantial promise as power generators and as solid-state Peltier coolers, attracting significant attention and positioning them as subjects ripe for further investigation. Categorized into alkali or alkaline earth, transition metal, and main-group chalcogenides, these materials and their respective subclasses are meticulously scrutinized to pinpoint the most suitable thermoelectric materials for specific applications with an optimal operational temperature span. In the quest for energy-efficient technologies characterized by simple designs, absence of moving components, and superior stability, thermoelectric materials play a crucial role. This review highlights the advancements in theoretical parameters as well as the figure of merit (ZT) of chalcogenide materials, emphasizing their device applications. These insights are intended to provide viable future approaches to mainstream thermoelectric materials. This review reveals that Cu_2Se achieves a maximum ZT value of 2.66 at 1039 K, marking it as the top performer among transition metal chalcogenides. Conversely, SnSe , a main-group metal monochalcogenide, exhibits a ZT value of 2.8 at 773 K, whereas nanowires of the main group of bismuth chalcogenides exhibit a ZT value of 2.5 at 350 K.

Keywords Chalcogenides · thermoelectric materials · monochalcogenides and dichalcogenides · pyrites · alkali or alkaline earth metal chalcogenides

Introduction

The depletion of natural resources is a consequence of the heavy use of nonrenewable energy sources such as coal and nuclear power in various fields. Thus, solar, wind, hydro, tidal, geothermal, and biomass energy are gaining traction to meet the increasing demand for electricity. Thermoelectric

(TE) energy, categorized as an “alternative energy,” utilizes temperature gradients to convert heat into electricity, thus aiding in recycling the prevalent waste heat.¹ Electricity is generated in TE power plants using heat from fossil fuels, solar panels, and industrial waste, thus promoting energy conservation and waste heat collection.^{2,3} Among other advantages, advanced TE technologies can greatly improve the energy efficiency of industrial infrastructure, cars, solar cells,⁴ electrochemical processes, catalysts, supercapacitors, nonlinear optics, thermal energy sensors,⁵ automotive waste recovery,^{6,7} wearable TE generators,⁸ aerospace applications,⁹ and nuclear detectors. They can be operated in a variety of temperature ranges, are inexpensive, and are less hazardous^{10,11} (Fig. 1). TE modules are smaller and lighter than other mechanical systems and operate without any moving components.¹² Their ability to heat and cool within a single module, combined with their precise temperature

✉ Ashwatha Narayana Prabhu
ashwatha.prabhu@manipal.edu

¹ Department of Physics, Manipal Institute of Technology, Manipal Academy of Higher Education, Manipal 576104, India

² Department of Physics, School of Applied Sciences, REVA University, Rukmini Knowledge Park, Yelahanka, Kattigenahalli, Sathanur, Bengaluru, Karnataka 560064, India

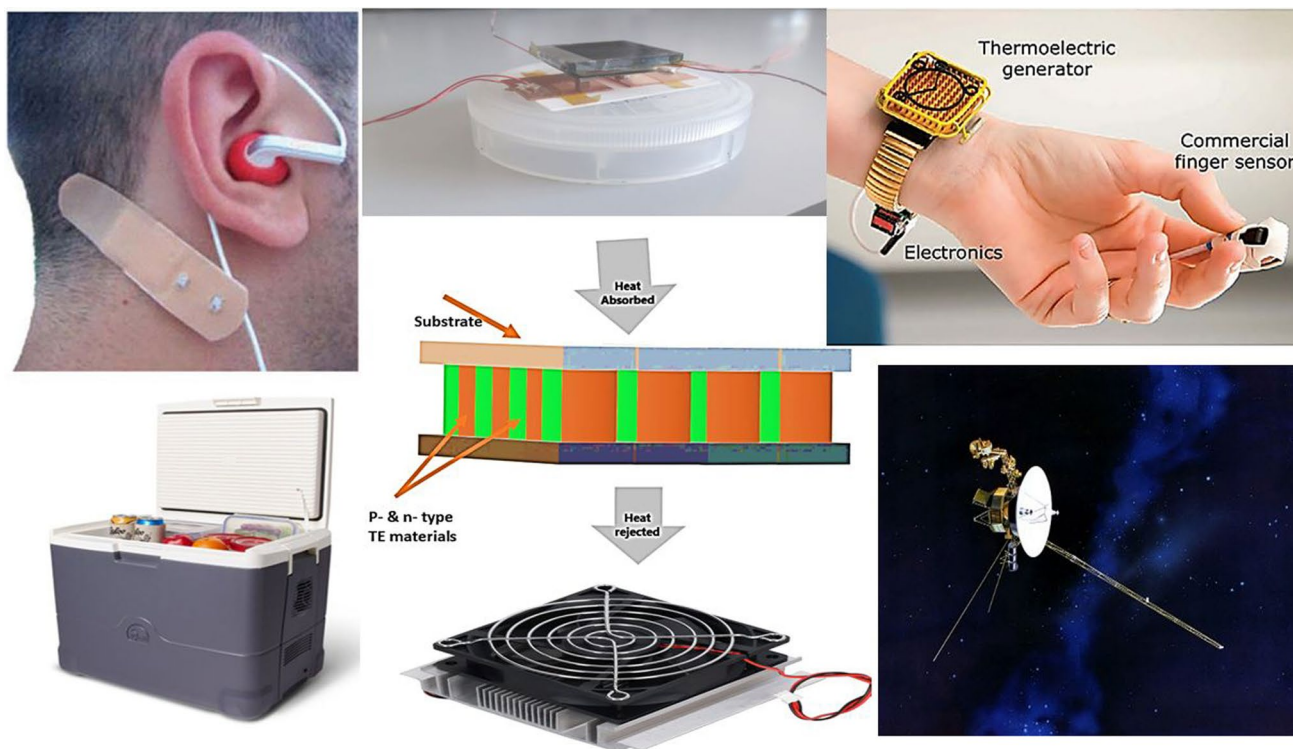


Fig. 1 Chalcogenide-based materials used in different applications such as flexible TE devices, electronics, CPU coolers, pacemakers, hearing devices, and space missions.

control, makes them extremely reliable. TE devices have environmental benefits, as they do not emit or rely on gases.

Chalcogenides are increasingly used in TE applications, acting as generators or refrigerators depending on their operating temperature.¹³ The figure of merit (ZT), a dimensionless quantity expressed by Eq. 1, is the most important aspect in determining the efficiency of TE materials¹⁴:

$$ZT = \frac{S^2 \sigma}{\kappa} T, \quad (1)$$

where $S^2 \sigma$ is the power factor (PF), in which S is the Seebeck coefficient, σ is electrical conductivity, and κ is thermal conductivity.

The current study focuses on chalcogenide materials specifically chosen for their high efficiency in TE applications, which is achieved through an improved PF and reduced κ , possibly through the use of materials with intrinsically low thermal conductivity and/or nanostructuring. In addition, novel approaches including nanocomposites, carrier filtering, low-dimensional materials, and phonon scattering are being investigated to improve the functionality of TE materials.^{15,16}

Among the various TE material systems studied, skutterudites have received substantial attention. Based on a prediction using a simple semiconductor transport model, a ZT

of 1.4 at 1000 K is expected, compared to 0.3 at 300 K.^{17,18} Despite its high PF, the lattice thermal conductivity of the original TE skutterudite CoSb_3 is very high (approximately $10 \text{ W m}^{-1} \text{ K}^{-1}$ for R.T), which reduces its efficiency. Filling voids in these materials with elements such as alkaline earth metals, alkali, group IV metals, and thallium has improved TE properties.^{13,14} Clathrates, with low-thermal-conductivity composition and open tetrahedral frames of Al, Ga, Si, Ge, or Sn, show promising ZT values. Electronic band structure studies of type I clathrates conducted using density functional theory (DFT)^{19–21} for optimal constitution of $\text{Sr}_8\text{Ga}_{16}\text{Ge}_{30}$ ²² and $\text{Ba}_8\text{In}_{16}\text{Sn}_{30}$ reveal ZT values as high as 0.5 and 1.7 at 300 K and 800 K, respectively. At 943 K, the optimized n -type clathrate $\text{Ba}_{24}\text{Ga}_x\text{Ge}_{100-x}$ ($x = 15$) achieved a ZT value of 1.25.²³ The intermetallic compounds of half-Heusler (HH) materials, including MNiSn ($M = \text{Ti, Hf, Zr}$), FeCrSb , RuCrSb , OsCrSb ,²⁴ and NbFeSb ,²⁵ are compounds of keen importance as promising high-temperature TE materials. A significant advancement was noted for the n -type $\text{Zr}_{0.5}\text{Hf}_{0.5}\text{Ni}_{0.8}\text{Pd}_{0.2}\text{Sn}_{0.99}\text{Sb}_{0.01}$, exhibiting a ZT value of 0.7 at 800 K.²⁶ A promising p -type compound, $\beta\text{-Zn}_4\text{Sb}_3$ has an incredibly low thermal conductivity at moderate temperatures. $\beta\text{-Zn}_4\text{Sb}_3$ at 670 K exhibits a considerably high ZT of 1.3.²⁷ The Si-Ge alloy used in deep-space mission radioisotope TE generator is a system with a discernible ZT at 1200 K. To optimize the TE performance of TE materials,

numerous substitutions of $\text{Yb}_{14}\text{MnSb}_{11}$ are made with alkali-earth, transition, and main-group metals.^{28,29} These materials are currently the primary focus in TE applications. Skutterudites, half-Heusler alloys, clathrates, and lead-based compounds are all excellent TE materials. However, they have disadvantages such as high cost, toxicity, and operating temperature.¹³ Recent investigations have confirmed that chalcogenides have consistently been selected as the best materials for such applications since the inception of thermoelectricity and will be increasingly used in the future. This assertion is supported by the continual improvement in the ZT value of chalcogenide materials, as depicted in Fig. 2. According to the results, the chalcogenide compounds are further investigated.

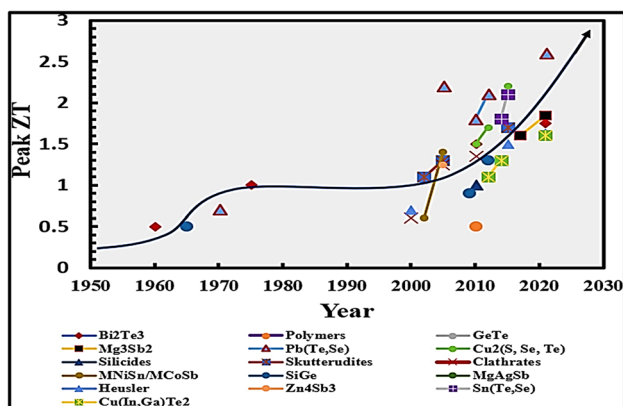


Fig. 2 Evolution of ZT for different high-performance TE material systems within their optimal temperature ranges. Reprinted from Ref. 30, under Creative Commons license CC BY.

This review highlights the superiority of chalcogenide materials over others, particularly sulfur (S), selenium (Se), and tellurium (Te), which are widely employed in TE generators^{31–34} and TE refrigerators. The main objective of the current review article is to evaluate various chalcogenide material branches, highlight their superior qualities, and determine the optimal operating temperature for each material. This article focuses on the application of chalcogenide materials in TE devices considering the improvements in their theoretical and experimental efficiency parameters (ZT) to date. These materials are categorized into three main branches: alkali or alkaline earth, transition metal, and main-group chalcogenides, and along with these, their subcategories are examined to determine the TE materials that are most suitable for applications (Fig. 3). This review article also aims to draw the readers' attention to content that has received little focus, namely groups such as alkali and alkaline material chalcogenides and transition metal chalcogenides, which can be further investigated to produce high-quality TE materials. The improvement in the efficiency of the materials with various preparation techniques is discussed.

TE Applications of Chalcogenide Materials

Han et al.³⁵ classified TE materials into nine groups based on their composition and structure. Bi_2Te_3 alloys, doped with Sb and Se, exhibited a ZT of 0.6 at 300 K and are widely used in TE refrigeration (groups 1–2). $\text{Bi}_2\text{Te}_3\text{-Sb}_2\text{Te}_3$ superlattice films exhibited a ZT of 2.4 at 300 K, stimulating nanomaterial exploration. Group 3 A-B-X (ternary) materials, such as polycrystalline CuGaTe_2 , achieved a ZT of 1.4 through ball milling and hot pressing, with the ZT reaching

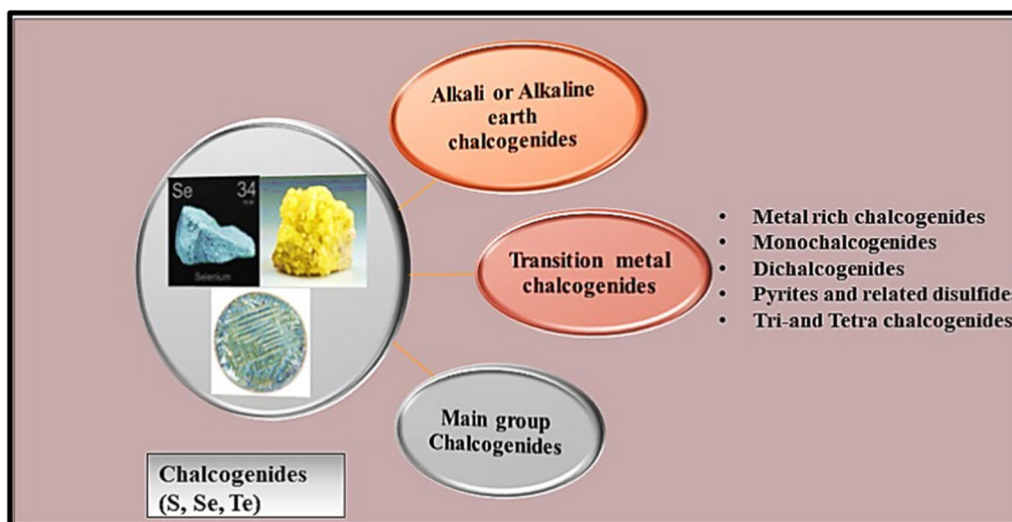


Fig. 3 Schematic showing the categorization of the chalcogenide material considered in this review

1.69 at 950 K^{36,37} Groups 4 and 5, Sn-X and In-X systems, offer high performance and affordability. Enhanced TE efficiency is achieved through elemental adjustments.³⁵ Owing to the interaction between the elements, $\text{In}_4\text{Se}_{2.78}$ and SnSe single crystals showed exceptional TE performance, with ZT values of 1.48 (n -type) at 705 K and 2 (p -type) at 923 K.³⁸ SnSe nanotubes revealed lattice thermal conductivity (κ_L) of $0.18 \text{ W m}^{-1} \text{ K}^{-1}$ at 750 K, a PF of $0.235 \times 10^{-3} \text{ W cm}^{-1} \text{ K}^{-1}$, and a ZT of 4.6 from first-principles calculations.³⁹ Group 6 materials with layered structures are effective TE materials due to their unique crystal structure and plane modulation. Tewari et al. and Gascoin et al. obtained maximum ZT values of 2 and 1 for CuCrS_2 and AgCrS_2 at 300 K and 848 K, respectively.^{40,41} A sandwich-like structure of the compound $(\text{AgCrSe}_2)_{0.5}(\text{CuCrSe}_2)_{0.5}$ exhibited a ZT of 1.4 at 773 K.⁴² Group 7 materials, including binary (e.g., GeTe), ternary (e.g., Ag-Sb-Te), and quaternary (e.g., Ag-Sb-Pb-Te or Ag-Sb-Ge-Te) compounds, are formed by phase separation, nucleation, growth, and spinodal breakdown. Zhang et al. created composites ($\text{Ag}_2\text{Te}/\text{Sb}_2\text{Te}_3$) with a ZT of 1.53 at 500 K through a nanodomain boundary-induced decrease in thermal conductivity.⁴³ The $[(\text{GeTe})_m(\text{AgSbTe}_2)]_{100-m}$ system, which is rich in GeTe, has extraordinary electrical conductivity, a high Seebeck coefficient, and relatively good thermal conductivity, but with defects such as metal vacancies and Te stoichiometry deviation. Group 8 comprises

binary or ternary Cu or Ag chalcogenides, with Cu_2Se and Cu_2S exhibiting remarkable TE performance. The α -phase of Cu_2Se exceeded 469.5,⁴⁴ whereas Nb-doped AgBiSe_2 exhibited a ZT of 1 at 773 K.⁴⁵ Group 9 includes Ga-Te systems such as Ga_2Te_3 , with low thermal conductivity, and non-layered transition metal chalcogenides such as MnTe , Ce_3Te_4 , CeSe_2 , and FeS_2 , which are promising for their complex crystal structures.

Synthesis of Chalcogenides

A multitude of diverse synthetic methods can be employed for the production of chalcogenides, including flux- and melt-based synthesis, vacuum/high-temperature deposition from the gas phase, hydrothermal synthesis, and solution-based synthesis. These techniques also include conventional direct-combination high-temperature methods. Innovative strategies include metal-nanoparticle-suspended alloy synthesis, the low-temperature synthesis of nanostructured metal oxides and chalcogenides, salt-inclusion synthesis, and various processes for synthesizing porous materials (Fig. 4). Traditional solid-state synthesis involves high-temperature (about 1273 K) direct reactions of pure elements mixed in appropriate stoichiometric ratios. Using the Bridgman method, Yamashita et al.⁴⁶ demonstrated that adding 8 wt.% excess Te provides p - $(\text{Bi}_{0.25}\text{Sb}_{0.75})_2\text{Te}_3$,

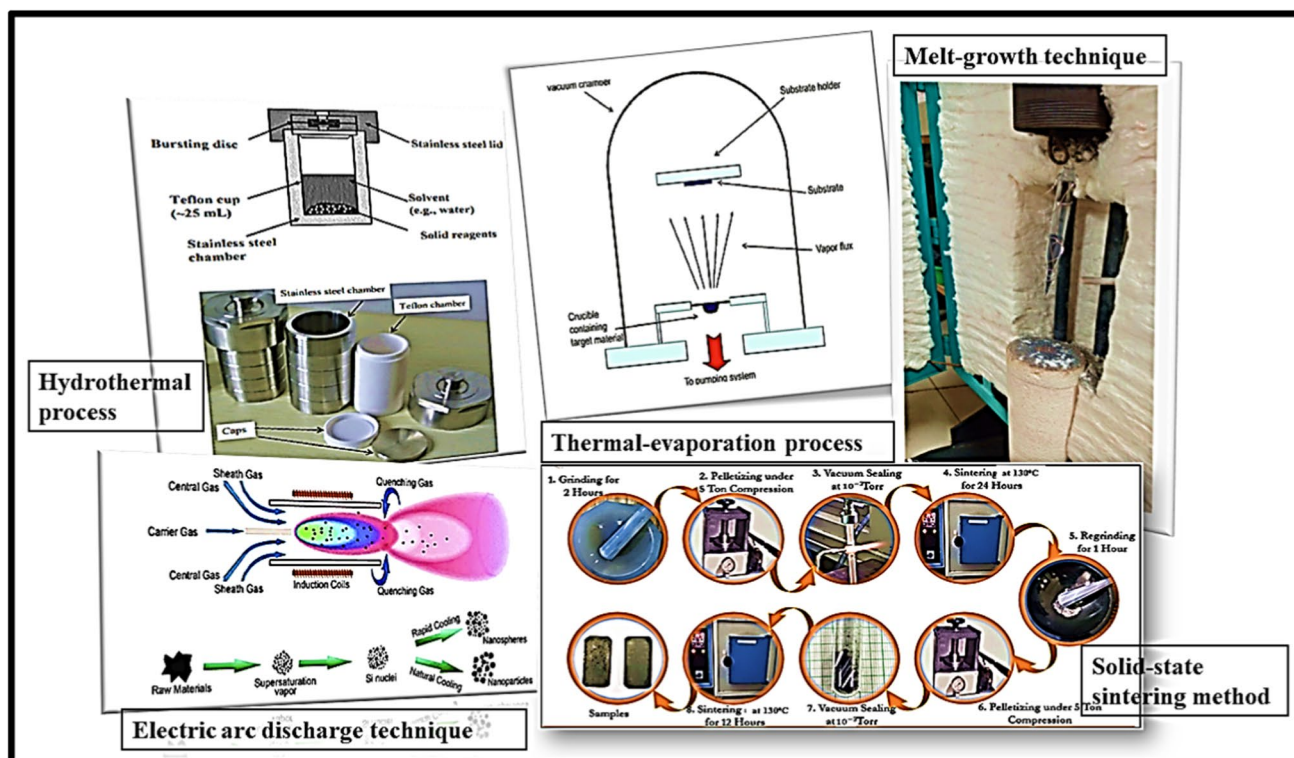


Fig. 4 Different synthesis methods for processing thin film, polycrystalline, and single-crystal materials.⁵¹

while 0.017 wt.% Te and 0.068 wt.% I-doping yield *n*-type $\text{Bi}_2(\text{Te}_{0.94}\text{Se}_{0.06})_3$. Annealing produced *ZT* values of 1.88 (*p*-type) and 1.59 (*n*-type) at 298 K for the two materials.⁴⁶ The modified Bridgman approach achieved a maximum *ZT* of 2.1 for SnSe-2SnTe with a PF of $\sim 5.5 \times 10^{-3} \text{ W m}^{-1} \text{ K}^{-2}$ at 793 K.⁴⁷ Similarly, $\text{Sn}_{0.95}\text{Se}$ was synthesized via a hydrothermal method at 873 K with a low PF value of approximately $0.777 \times 10^{-3} \text{ W m}^{-1} \text{ K}^{-2}$.⁴⁸ Multilayer Mo-SnSe films and 2.6 at.% Mo-doped SnSe films, produced via magnetron sputtering, exhibited a PF of $0.44 \times 10^{-4} \text{ W m}^{-1} \text{ K}^{-2}$ at 576 K, outperforming undoped SnSe films due to the heterojunction.⁴⁹ Melting and ball milling improved the TE properties of aluminum-doped Cu_2Se ($\text{Cu}_{1.94}\text{Al}_{0.02}\text{Se}$), achieving *ZT* of 2.62 at 1039 K. However, these materials are less suitable for low-temperature applications.⁵⁰

Alkali or Alkaline Earth Metal Chalcogenides and Their TE Applications

Alkaline metal chalcogenides and alkaline earth compounds crystallize in an antiferroite structure resembling sodium chloride.⁵² Rare-earth chalcogenides exhibit a variety of physical properties, particularly in quaternary systems. Te-rich alkali metal tellurides have distinct structural and transport characteristics. Rare-earth chalcogenides (e.g., RX_2 , R_2X_3 , R_3X_4 , and RX) exhibit mixed valence effects, differing significantly from oxides and necessitating different handling methods.

Alkali metal carbon nanotubes (AM-CNTs) are considered promising TE materials due to their notable electrical conductivity, whereas doped semiconducting single-walled CNTs (SWCNTs) are recognized for their exceptional Seebeck coefficient. Despite the considerable attention received by carbon nanotubes doped with *p*-type materials, their *n*-type variants have lagged,^{53,54} primarily due to concerns regarding their stability. Dorling et al.⁵⁵ introduced a carbon nanotube dissolution technique, enabling the production of *n*-doped films. These films exhibit a favorable Seebeck coefficient in addition to high electrical conductivity, making them appealing candidates in the realm of TE applications.⁵⁵ The hybrid system, which combines an alkali metal TE converter (AMTEC) and a segmented TE generator (STEG), shows promise for thermal-to-electric conversion. This technology has sparked significant interest due to its potential for home, military, and aerospace applications.⁵⁶ AMTEC has limitations such as 15% conversion efficiency and time-dependent power depreciation. Research on novel electrode materials^{56,57} and enhanced manufacturing techniques can address these issues.⁵⁸ Some alkali-based TE materials have shown good TE performance, as listed in Table I below.

In the creation of TE materials, heavy components in narrow-bandgap semiconductors are commonly used.

Tellurides, in particular semiconducting lanthanum chalcogenides, are prominent in TE investigations and hold promise for high-temperature applications.⁶⁶ A detailed analysis presented in Table I shows the energy bandgap, Seebeck coefficient, electrical conductivity, and *ZT* values of calcium chalcogenides at specific temperatures, as obtained from DFT calculations. Although showing satisfactory results through theoretical studies, the alkali and alkaline earth metal chalcogenides have not yet seen any practical applications apart from AMTEC. The reason for these failures could be the high reactivity and oxidation properties of these elements when exposed to the atmosphere. In addition, alkali metals are good conductors of heat, which makes them less suitable for TE applications where the phonon-glass electron-crystal approach is important. Therefore, focusing on these branches of materials is imperative in order to bring them into TE material application.⁶⁷ So far, these materials have been widely used as guest materials⁶⁸ to modify the electronic structure of existing TE materials and enhance their performance.

Transition Metal Chalcogenides and Their TE Applications

Transition metal chalcogenides (TMCs) are monochalcogenides or dichalcogenides with the general formula M_mX_m , where M represents transition metals (Sc, Ti, V, Cr, Mn, Fe, Co, Ni, Cu, and Zn) and X represents layered or unlayered S, Se, and Te. The most widely studied ultrathin materials besides graphene and hexagonal boron nitride (h-BN) are TMCs.⁶⁹ The layered structure of TMCs, which differs in its electrical and chemical properties from bulk semiconductor material, is one of its most notable characteristics. Sulfides, selenides, and tellurides are only a few of the key structural types that the TMCs represent. Typically, binary stable layered crystal formations are created when transition elements from groups IV to VII-B combine with elements from group VI-A, such as S, Se, and Te. The usual formula for these layered TMCs consists of a transition metal atom from group IV-B (Ti, Zr, Hf), group V-B (V, Nb, Ta), group VI-B (Mo, W), or group VII-B (Tc, Re), plus a chalcogen atom from group VI-A (S, Se, Te). Except for the bandgap (E_g), which depends on the chemical combination, the total number of layers, and whether adoption of atoms is present, the bulk structure and features of TMCs almost exactly mimic semimetal pure graphene. The E_g of TMCs ranges between 0 eV and 2 eV. The E_g in sulfides is normally 1–3 eV, although it decreases in selenides and nearly disappears in tellurides. For group VI transition metal dichalcogenides (TMDs) that consist of tungsten disulfide (WS_2), molybdenum disulfide (MoS_2), and molybdenum diselenide

Table 1 Properties of TE materials based on alkali or alkaline earth metals^{59–65}

Material	Model	Temperature (K)	Energy band-gap (eV)	Seebeck coefficient ($\mu\text{V K}^{-1}$)	ZT
CaO-rock salt	DFT + BTE	1200	3.691	275	0.7
CaO-hexagonal			2.489	150	0.5
CaS-rock salt	DFT + BTE	1200	2.409	175	0.6
CaS-hexagonal		225	3.163	300	1.35
CaSe-rock salt	DFT + BTE	1200	2.061	185	0.7
CaSe-hexagonal		510	3.028	350	1.45
CaTe-rock salt	DFT + BTE	1200	2.602	150	0.4
Na ₂ Te (<i>p</i> -type)	DFT + BTE	300	2.48	123	0.25
Na ₂ Te (<i>n</i> -type)	DFT + BTE	300	2.48	25	0.11
SrCdSnS	DFT + BTE	800	3.25	−94	0.019
SrCdSnSe	DFT + BTE	800	3.00	−10	0.60
SrCdSnTe	DFT + BTE	800	1.90	53	0.09
NaBiSe ₂	Experiment	596	–	−510	0.025
NaBi _{0.75} Sb _{0.25} Se ₂		596	–	−250	0.24
NaBi _{0.5} Sb _{0.5} Se ₂		596	–	−550	0.01
Na ₂ GeS ₃	DFT	1000	2.5	300	0.92
Na ₂ GeSe ₃	DFT	1000	2.3	400	0.90
Na ₂ GeTe ₃	DFT	1000	1.5	700	0.85
MgDy ₂ S ₄	DFT	600	–	900	–
MgDy ₂ Se ₄	DFT	600	–	400	–
CsAg ₅ Te ₃	DFT	727	0.67	650	1.40
CsAg ₅ Te ₃	SPS	673	–	240	0.67

DFT density functional theory, *BTE* Boltzmann transport equations, *SPS* spark plasma sintering

(MoSe₂), numerous instances of phase alteration owing to chemical interactions have been observed. These materials might be essential for upcoming studies as well as practical applications.⁷⁰ Ternary metal chalcogenides are a suitable substitute for hazardous binary metal chalcogenides, such as cadmium chalcogenides. The most difficult compounds to produce are those with the general formula $M_xM'_yM''_zX_n$ (M = transition metal, M'/M'' = transition or other metal, and X = S, Se, or Te). In terms of their electrical, chemical, and thermal properties, many TMCs may form crystals with layers that are more anisotropic than graphite. Groups IV through VII of the TMCs frequently have a hierarchy system, whereas groups VIII and X usually have non-layered structures. Due to their distinct characteristics, single-layer TMDs are ideal for research in both fundamental and technologically significant fields.⁷¹ The typical structure of TMDs is shown in Fig. 5.

As a result of the low thermal conductivity (κ) and high Seebeck coefficient (S), the TMCs have also been explored for their distinctive geometry and electrical properties as good TE candidates. These applications are described in more detail below. The TMCs are subdivided into five groups, namely, metal-rich chalcogenides, monochalcogenides, dichalcogenides, pyrites, and tri- and

tetra-chalcogenides. A detailed description of each subdivision is provided below.

Metal-Rich Chalcogenides

The late lanthanides and early transition metals contain the vast bulk of metal-rich chalcogenides (Sc, Y, and Ti).⁶⁹ Chalcogenide monolayers end up with numerous thick blocks of transition metal atoms in the intriguing family of solid-state structures known as transition-metal-rich chalcogenides.⁷³ Ta₂Se, the earliest transition-metal-rich chalcogenide, was prepared using the arc-melting procedure. Ta₂Se is the intercalation of two layers of Se between every four layers of Ta. DFT-based full-potential linearized-augmented plane wave computations were used to analyze the structural, electrical, optical, and thermodynamic characteristics of ScX (X = S, Se, and Te) and the associated ternary alloys.⁷⁴ In transition-metal-rich chalcogenides, the transition metal frequently adopts the anti-format of TMDs, taking the form of an octahedron or trigonal prism with chalcogen elements at the center.⁷⁰ Figure 6 illustrates the interaction process between metals and chalcogenides.

The high inherent conductivity of metal-rich chalcogenides negates the need for additional conductive materials

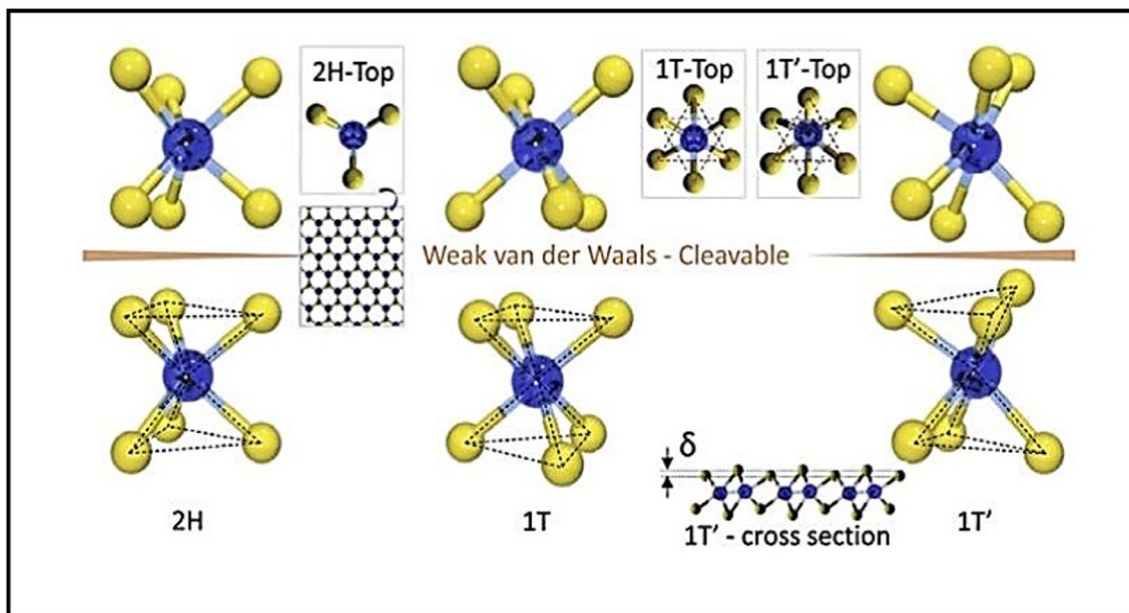


Fig. 5 Typical structures of layered TMCs. Cleavable 2H, 1T, and 1T0 structures in a layered TMD are shown. Reprinted with permission from Ref. 72. Copyright 2019, Royal Society of Chemistry.

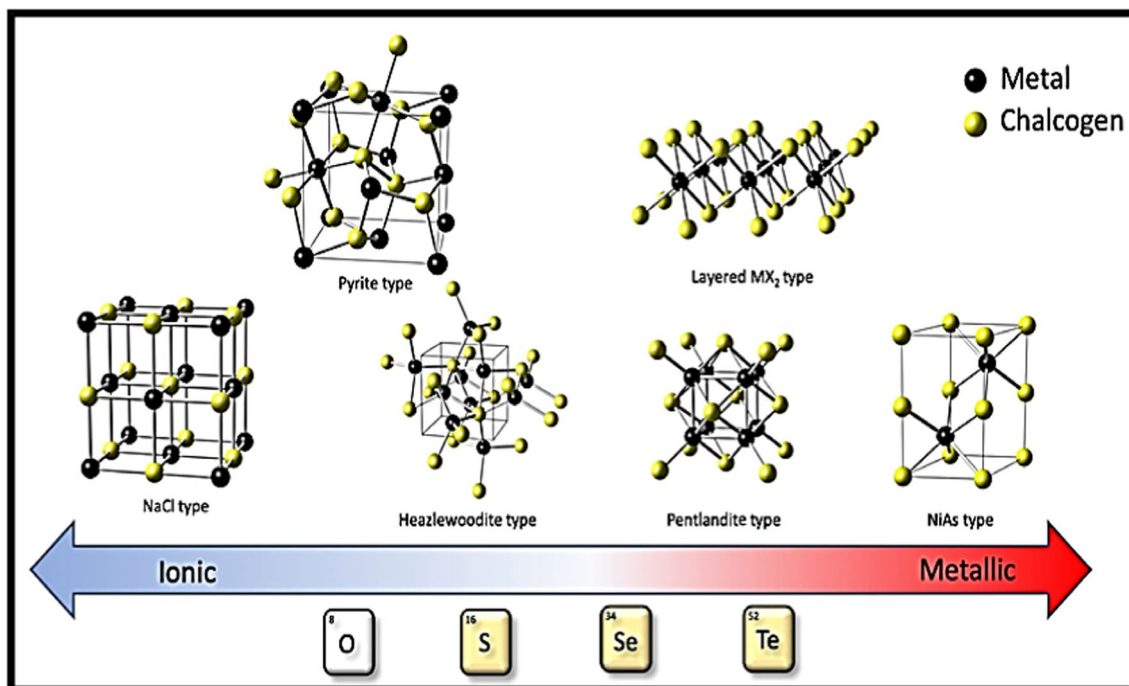


Fig. 6 Common structural motifs of metal chalcogenides. The dominant structural motifs can be understood as primarily ionic, metallic, or motifs in between these two extremes. Reprinted from Ref. 75, under Creative Commons license CC BY.

or sophisticated nanostructuring, in contrast to chalcogen-rich metal chalcogenides. Less research has been devoted to metal-rich chalcogenide materials than to the huge family of stacked TMDs. Metal-rich chalcogenides are anticipated to be crucial in upcoming scientific research and commercial

applications.⁷⁰ As TE materials, metal-rich chalcogenides have also been studied, but not extensively. The TE properties of these materials require further analysis before being used as TE materials. There are a few materials such as nickel antimonide telluride or selenide, complex silver

tellurides, and palladium selenide which exhibit TE properties, as presented in Table II.

Transition Metal Monochalcogenides

Compounds such as TiX and MnX , where $X=O, S,$ or Se ; and VS and $Sc-S$ with $S=S$, are examples of transition metal monochalcogenides (TMMs). It is challenging to produce chemically separate TMMs, the 1D vdW-wired materials.⁷⁹ Recently, bulk $MoTe_2$ was successfully vacuum-annealed to create $MoTe$.⁸⁰ Most of the time, TMMs were found in mixtures with bulk TMDs or in bundles, making it difficult

Table II Properties of TE materials based on metal-rich chalcogenides^{76–78}

Material	Power factor ($W m^{-1} K^{-2}$)	Seebeck coefficient ($\mu V K^{-1}$)	Temperature (K)	Resistivity (Ωm)
Pd_5InSe	0.5×10^{11}	–	300	5.25×10^{-21}
Pd_8In_2Se	2.75×10^{11}	–	300	2.30×10^{-21}
$Ni_{5.66}SbTe_2$	4.11×10^{-18}	–	300	1.4×10^{-10}
$RbAg_3Te_2$	–	700	350	–
$Rb_2Ag_3InTe_4$	–	350	350	–

to characterize their unique features. Researchers working to understand the nature and possible uses of the vdW-wired materials still face a substantial hurdle in the manufacturing of single-wired TMMs.⁸¹

A simple procedure for separating $MoTeNWs$ with well-defined atomic structures was developed by using a CNT template for self-assembly. Complex structural dynamics were observed in a single $MoTeNW$ within a CNT; this has never been observed in bundled $MoTeNWs$.⁸³ Mo_2TeS and Mo_2TeSe , the other two TMMs, showed similar robustness and topological feature modification under external load. M_6X_6 ($M=Mo$ and W ; $X=S, Se,$ and Te) 1D metallic TMM nanowires exhibited structures and intrinsic anisotropic metallic characteristics that make them potential candidates for nanodevices.⁸⁴ Using a first-principles calculation, Gao et al. showed that the hole-free $CuSe$ has the Dirac nodal line fermion (Fig. 7), which was subsequently produced on the surface of $Cu(111)$ via molecular beam epitaxy (MBE) and has promising characteristics.⁸⁵ Chin et al.⁸² demonstrated the use of a planarized solid-state chemical reaction to produce ultrathin 2D TMMs. Even though the results are promising, these materials are still in their infancy, and their fabrication challenges make it difficult to apply them in practical applications. Monochalcogenides, which are transition materials, must be manufactured using practical methods for their application in devices.

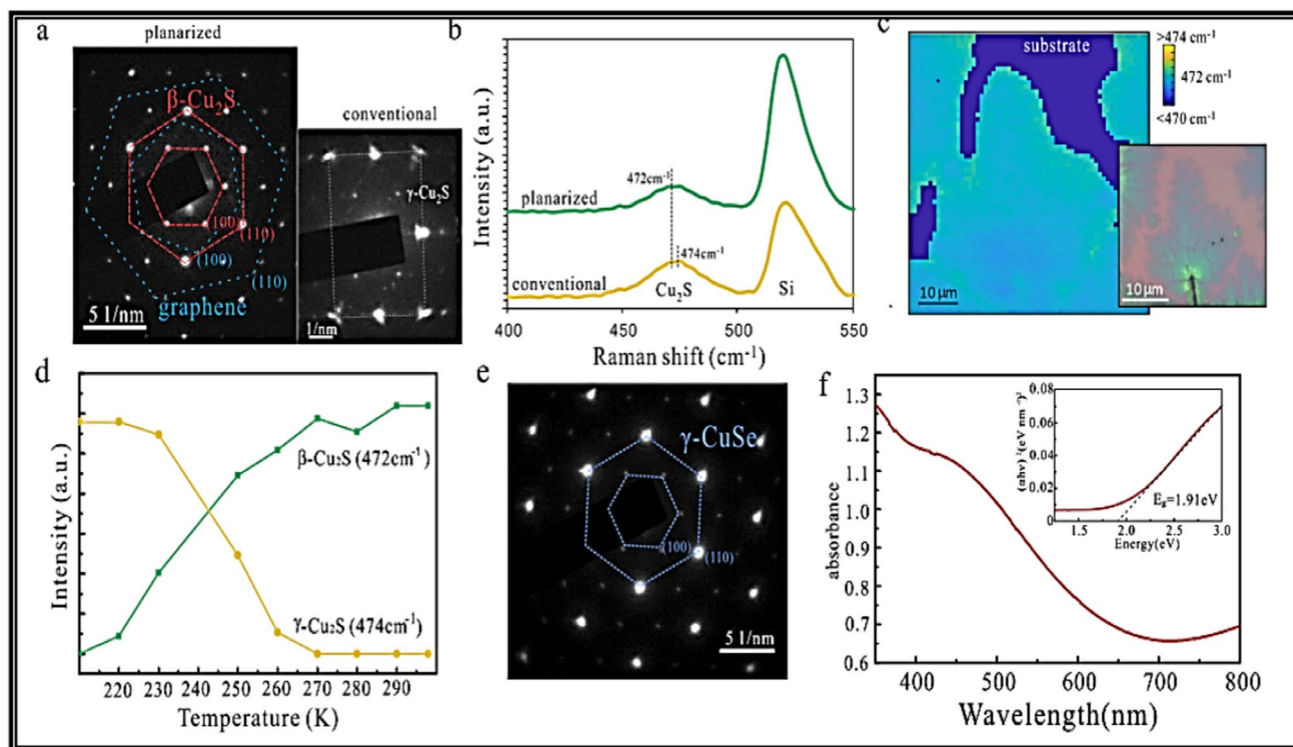


Fig. 7 Features of 2D crystals grown by planarized reaction: selected area electron diffraction (SAED) and Raman spectra for Cu_2S grown under planarized growth conditions can be seen. Reprinted from Ref. 82, under Creative Commons license CC BY.

It can be seen through a literature survey that out of the various transition metals, Cu and Ag have been explored to a greater extent, leaving room for exploring the other materials from this branch.^{89,116,117} The TE properties of the transition-metal-based materials are shown in Fig. 8, and some are tabulated in Table III. The investigation shows that Cu-based chalcogenide materials, which exhibit peak performance in the mid- to high-temperature range, are promising candidates for use in TE generators. In contrast, Ag-based materials with high ZT values within the ambient temperature range, emerge as optimal choices for Peltier coolers. Further, Al-doped ZnO ($\text{Al}_{0.02}\text{Zn}_{0.98}\text{O}$), although an oxide material, exhibits the highest ZT of 0.3 at 1000 K.^{118,119} By using a void-forming agent, namely carbon nanoparticles or organic polymers, a distinct type of Al-doped ZnO has exhibited elevated ZT of 0.4 at 773 K (shown in Fig. 9). Complex crystal structures^{120–122} are formed by the quaternary chalcogenide materials, which are beyond the scope of this review article and therefore are not discussed here.

Transition Metal Dichalcogenides

Because of the wide range of fascinating properties of TMDs and their potential use in developing technologies, research on these materials is likely to remain important. A TMD consists of a metal (M) sandwiched between two atomic layers of chalcogen (X). The typical atomic ratio in multi-layer TMDs to produce MX_2 is one transition metal to two chalcogen atoms, with a few exceptions: 1:1 metal chalcogenide (MX) and 2:3 quintuple layers (M_2X_3). Within the chalcogen–metal–chalcogen configuration are weak van der Waals (vdW) connections between every chalcogen–chalcogen layer in the z -direction, and these contacts are one layer. For metal dichalcogenides, the oxidation state is +4, and for chalcogenides, it is -2 .^{124,125} The structure of 2D TMDs can be classified as trigonal prismatic (hexagonal, H), octahedral (tetragonal, T), or distorted phase depending on the arrangement of atoms (Fig. 10).¹²⁶

TMDs are particularly well suited for TE applications due to their very high electrical conductivity and comparatively moderate thermal conductivity.¹²⁵ The ideal temperature

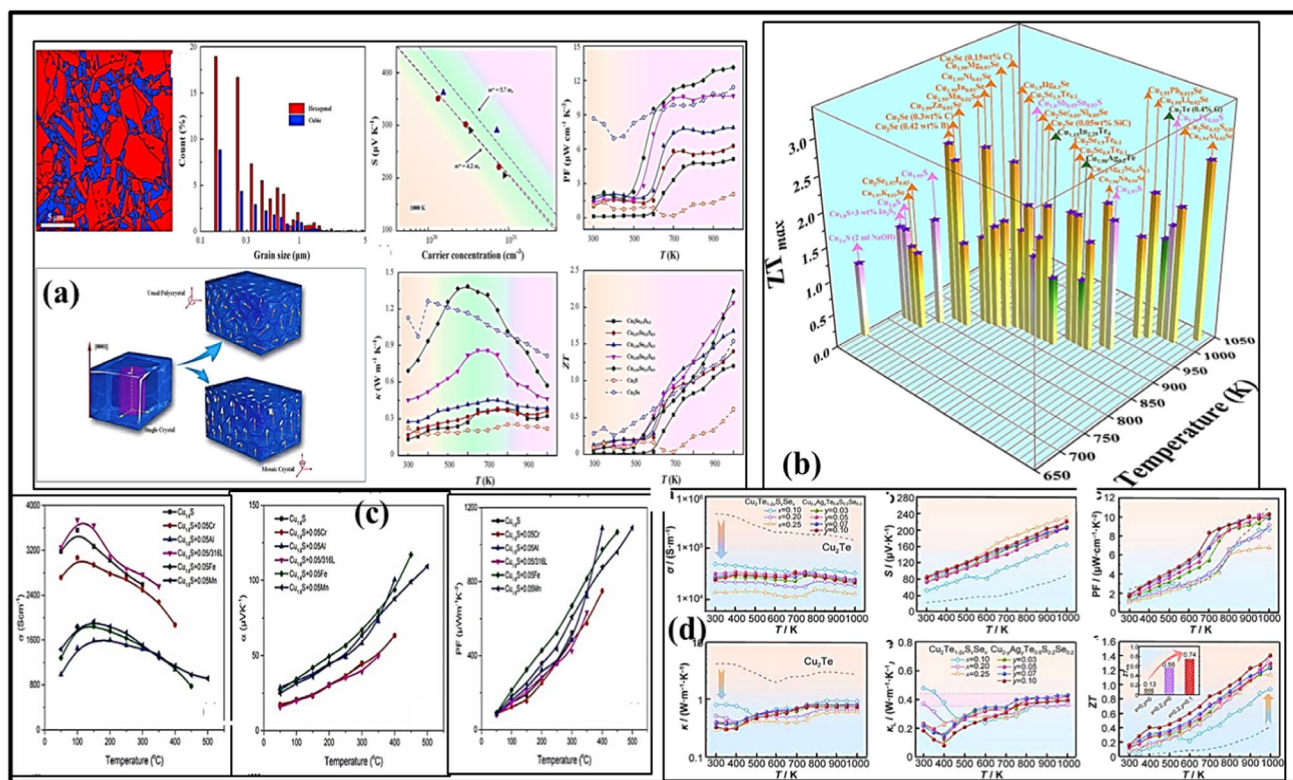


Fig. 8 (a) Phase mapping grain size distribution, structural characteristics of single-crystal, polycrystalline, and mosaic crystal materials, dependence of S on Hall carrier concentration at 1000 K, temperature dependence of PF, κ , and ZT of Cu–Se–S compounds. Reprinted with permission from Ref. 86. Copyright 2024, Springer Publishing Company. (b) Temperature-dependent ZT for Cu_2S -, Cu_2Se -, and Cu_2Te -based liquid-like TE materials. Reprinted with permission from

Ref. 87. Copyright 2023, CC BY 4.0, Wiley. (c) Changes in electrical conductivity (σ), Seebeck coefficient (S), and PF as a function of temperature of Cu_2S using different elements for reducing the oxidation and thermal decomposition. Reprinted with permission from Ref. 88. Copyright 2024, Elsevier. (d) Temperature-dependent TE properties of $\text{Cu}_2\text{Te}_{1-2x}\text{S}_x\text{Se}_x$ and $\text{Cu}_{2-y}\text{Ag}_y\text{Te}_{0.6}\text{S}_{0.2}\text{Se}_{0.2}$ samples. Reprinted with permission from Ref. 88. Copyright 2024, Elsevier.

Table III Transition-metal-based TE materials and their TE properties

Material	Preparation method	Thermal conductivity (W m ⁻¹ K ⁻¹)	ZT	Temp (K)	References
α -Cu ₂ Se	–	0.5	1.5	1000	89
Cu ₂ Te	Annealing	~1.2	1.1	1000	90
α -Ag _{1-x} CuSe	Solid-state reaction	~0.5	0.9	693	91
β -Cu _{2-x} Se	–	1.2	1.5	1000	89, 92
Cu ₂ Se-MWCNT (1%)	Reduction method	–	–	450	93
Cu ₂ S	Ball milling	–	1.5	450	88
Ag ₂ Te nanoparticles	Hydrothermal method	0.45	1.7	373	94
Cu _{1.97} S	SSR + SPS	0.48	1.63	1000	95
Cu _{1.9} Mn _{0.1} S	SSR + MA + SPS	1.25	1.41	700	96
Cu _{2-x} S	HP	0.62	1.23	710	97
Cu _{1.8} Sb _{0.02} Sn _{0.03} S	MA + SPS	0.6	1.1	773	98
Cu _{1.8} Na _{0.05} S	MA + SPS	0.76	1.04	773	99
Cu _{2-x} S-0.25%C	WC + SPS	0.47	1.01	773	100
Cu _{1.96} S	HTS + MA + SPS	0.68	1.00	773	98
Cu _{1.8} S-1%Ru	MA + SPS	1.05	2.4	773	101
AgCuSe _{0.6} S _{0.4}	Melting-annealing	–	0.53	300	102
Ag _{3.96} SeS	Melting	0.62	0.73	493	103
(Ag _{0.99} Cu _{0.01}) ₂ SeS _{0.01}	Melting	1.14	0.45	372	104
Ag ₂ Se + 5 mol.% nano-Cu ₂ Se	Melting + SPS	2	0.7	875	105
Ag ₂ Se + 5 mol.%ZnSe	MA + SPS	1.2	–	383	105
Ag ₂ Se + CuAgSe + PEDOT + nylon substrate	Thin film	0.46	1.2	300	106
Ag ₂ Se + SWCNTs + nylon substrate	Thin film	–	1.56	300	107
Ag ₂ Se on PI substrate	Thin film	0.66	1.1	300	108
Cu ₂ S Powder	M + SPS	–	2.7	800	109
Cu ₂ Se _{1.015} /0.1 mol.% BiCuSeO	M + SPS	–	2.1	973	110
Cu _{1.96} Na _{0.04} Se micro-pores	HM + HP	–	0.3	973	111
Cu ₂ Se _{0.7} Te _{0.3} solid solutions	BM + CP	–	1.47	500	112
Cu ₂ Te-0.4 graphene (composites)	M + SPS	–	1.25	1000	113
ZnO	Solid-state reaction	–	0.06	1100	114
PtPS	DFT	–	0.3	300	115
PtPSe	DFT	–	0.4	300	115
PtPTe	DFT	–	2.5	300	115

SSR solid-state reaction, SPS spark plasma sintering, MA mechanical alloying, HP hydraulic pressing, WC wet chemical synthesis, HTS or HS hydrothermal synthesis, M melting, HM hydrothermal method, BM ball milling

range for using TMDs as TE systems is between 600 K and 1000 K, where the ZT values of these compounds vary from 0.1 to 0.6. The band structure of the materials is linked to TE values found in the TMD single-crystal flakes and films, which represent the inherent transport abilities of the material. Therefore, flake samples offer a perfect environment for investigating the TE capabilities of these materials. Highly aligned and dense polycrystalline materials may be capable of conducting electricity and TE transport capabilities that are quite like those of their single-crystal counterparts. The TE properties in TMDs have been studied primarily in MoS₂, although other materials such as TiS₂, WSe₂, PtSe₂, and 1T-MoTe₂ have also been the subject of study.

Improved TE performance in TMD superlattices has been achieved by utilizing phonon scatterers and a blend of materials that have various structural and transport properties as interfaces. The TMD samples have been generated as nanoflake complexes through liquid-phase exfoliation and restacking using drop casting or inkjet printing because vdW bonding is weak. Chemically exfoliated WS₂ and NbSe₂ nanosheet assemblies allow for the practical development of a flexible TE generator using TMDs.¹²⁸ These TMDs, which have PF values of 0.005–0.007 × 10⁻³ W m⁻¹ K⁻² in *n*-type WS₂ and 0.026–0.034 × 10⁻³ W m⁻¹ K⁻² in *p*-type NbSe₂, are the ideal values for nanosheet assemblies. A concept for a

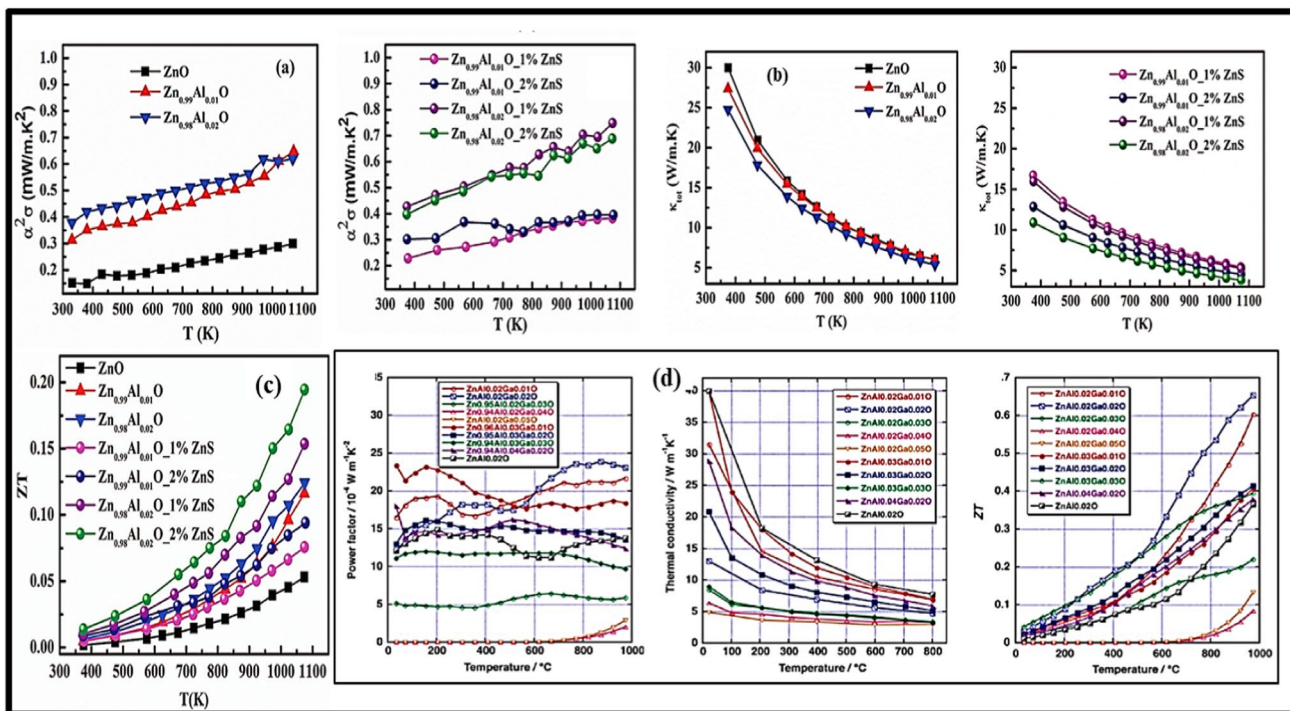


Fig. 9 Temperature-dependent TE properties: (a) power factor, (b) total thermal conductivity, and (c) ZT of Al-doped and ZnS-coated ZnO materials. Reprinted with permission from Ref. 114, Copyright

2024, Wiley. (d) TE properties such as PF, κ , and ZT of Al-Ga-codoped ZnO samples. Reprinted with permission from Ref. 123. Copyright 2023, CC BY 4.0.

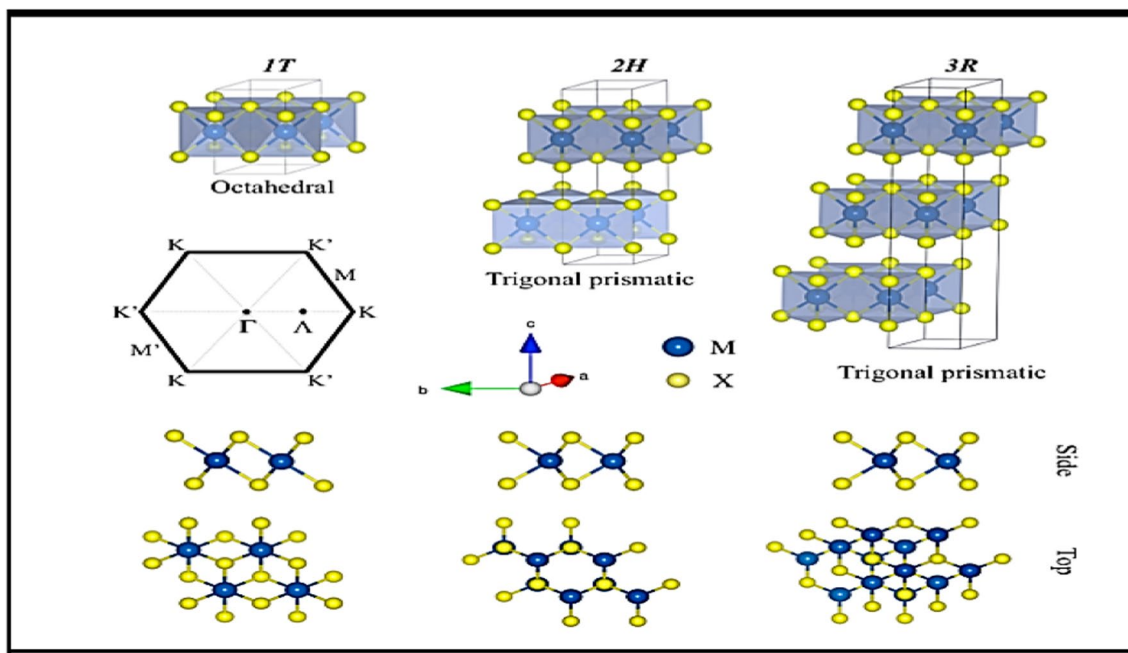


Fig. 10 Structure of TMCs having a composition of the form MX₂. Depending on the metal atom, the MX₂ family can crystallize in 1T (tetragonal), 2H (hexagonal), or 3R (rhombohedral) symmetry. The

figure also shows the hexagonal Brillouin zone with the high-symmetry *k* points. Reprinted with permission from Ref. 127, under Creative Commonslicense CC BY.

TMD-based solid-state thermionic appliance, which might serve as a generator or refrigerator, was also proposed. The method used a vdW heterostructure with two TMDs (WSe₂ and MoSe₂) and two electrodes made of graphene.

TMDs have significantly lower thermal conductivity than graphene, making them suitable for high-performance TE applications. It would be intriguing to create TMD-based wearable electronic devices that use the temperature difference between the human body¹²⁹ and the surrounding air to generate power.⁸ MoS₂ with reduced graphene oxide nanocomposite (MoS₂-RGO) enhanced the TE performance of molybdenum disulfide by 5920%. TE enhancements were made possible by the MoS₂-RGO nanocomposites largely due to their improved electrical conductivity, enhanced Seebeck effect, and concomitant reduction in the thermal conductivity of MoS₂.

In *p*-type and *n*-type MoS₂ and WSe₂, the *ZT* was projected as being close to unity (*ZT* values for some of the TMD materials are given in Table IV), varying according to the number of atomic layers, and achieved the optimal value for one or two monolayers (MLs). To attain a remarkable *ZT* of 1.87 at 800 K, it was discovered that the thickness of the SnS₂ nanosheet was reduced to approximately three MLs, where *S* and σ along the in-plane directions would increase and κ would decrease. The band structure and TE characteristics were tuned by varying the thickness from one to four MLs for MoS₂, MoSe₂, WS₂, and WSe₂. The predictions for the TMD heterostructure were equally promising. In the

MoS₂/WS₂ hybrid nanoribbons,¹³⁰ it was anticipated that the MoS₂/WS₂ contact would result in a *ZT* of 5.5 at 600 K by decreasing the lattice thermal conductivity more than electron transport. Glassy phonon transport and interface scattering in the ML ZrSe₂/HfSe₂ superlattice implied strong *n*-type PFs with substantial electronic band degeneracy. Calculations for the *ZT* obtained a value of 5.3 in the *n*-type superlattice at 300 K and 3.2 in the *p*-type superlattice. The *p*- and *n*-type doping predicted *ZT* values of 1.1 and 0.3, respectively, at 300 K, and even as large as *ZT* > 4 at 800 K for exceptionally thin BP/MoS₂ bilayers.¹²⁸

TMDs might outperform graphene in the field of thermoelectricity because of their low thermal conductivity, high effective mass, valley degeneracy, adaptable and programmable transport characteristics, band structure sensitivity, and confinement-sensitive phonon spectrum. In addition, due to their unusual electrical characteristics and customizable band structure, TMDs have sparked widespread interest as possible TE materials.¹⁴⁰ Recent research has looked into numerous techniques for improving the TE performance of TMDs. Theoretical calculations and computational modeling are critical in predicting and understanding the TE characteristics of TMDs, directing experimental efforts toward their material design and optimization. Current research focuses on the integration of TMD-based TE modules into practical devices such as waste heat recovery systems,¹⁴¹ wearable energy harvesters,¹⁴² and portable cooling systems.^{143,144} Despite these advances, problems such as improving their

Table IV TE properties of some of the TMD systems

Sample	Compound type	Power factor (W m ⁻¹ K ⁻²)	<i>ZT</i>	Temp (K)	References
Highly oriented polycrystalline TiS ₂ with Cu intercalation	Polycrystalline	1.7 × 10 ⁻³ at 325 K	0.45	800	131
rGO-MoS ₂ and rGO-WS ₂ composites	Composite prepared from liquid-phase exfoliation	–	0.022–0.025	300	131
1T-MoS ₂ /PEDOT:PSS composite	Composite prepared from liquid-phase exfoliation	–	0.04	300	131
TiS ₂	–	0.371	0.16	300	131
TiSSe	DFT	–	1.04	300	132
TiSTe	DFT	–	0.95	300	132
TiSeTe	DFT	–	0.88	300	132
CuSbS ₂	Bridgman technique	0.01152 × 10 ⁻⁴	0.988	503	133
CuGaTe ₂ + Sb alloying	Alloying	–	0.33	300–623	134
CoTe ₂	Vacuum solid-state reaction	330 × 10 ⁻⁶	3.7 × 10 ⁻²	619	135
NiTe ₂	Vacuum solid-state reaction	80 × 10 ⁻⁶	4.4 × 10 ⁻³	617	135
FeTe ₂	Vacuum solid-state reaction method	–	1.3 × 10 ⁻²	617	135
FeTe ₂	–	–	1.57 × 10 ⁻²	373	136
Fe _{0.5} Co _{0.5} Te ₂	SPS	–	0.18	600	137
Ag _{0.7} Sb _{1.12} Te ₂	Arc-melting	0.6	0.61	750	138
AgSbTe ₂	Hg doping	–	–	570	139

DFT density functional theory, SPS spark plasma sintering

overall TE efficiency, boosting the stability and dependability of TMD-based devices, and lowering the production costs for large-scale applications still remain. Nonetheless, recent research indicates that TMDs show great promise as TE materials and will play an important role in the future of energy harvesting and thermal control systems.

Pyrite and Related Disulfides

Pyrite, an iron disulfide with the formula FeS_2 , is commonly referred to as “firestone.” One well-known example of a cubic structure type with the general composition AB_2 is the mineral pyrite. Pyrite is classified as a semiconductor due to its bandgap of 0.95 eV. Pure pyrite is intrinsically *n*-type in both its crystal and thin-film forms. This is most likely due to sulfur vacancies acting as *n*-dopants in the pyrite crystal structure. Among the advantages of this material are its abundance, nontoxic nature, low cost, high quantum efficiency, and increased optical absorption coefficient. The interatomic separations in disulfides including pyrite structures were studied by Birkholtz et al.¹⁴⁵ The sulfur atoms are arranged in pairs along the trigonal axis of the lattice, with each sulfur atom situated approximately 3/8ths of the diagonal length away from a metal atom (Fig. 11).

Gudelli et al.¹⁴⁶ investigated the electronic structure and TE properties of the marcasite (m) and synthetic pyrite (p) phases of FeX_2 ($\text{X} = \text{Se}, \text{Te}$) using the Boltzmann transport equation and first-principles DFT. Except for marcasite FeTe_2 , which was more favorable to electron doping, the

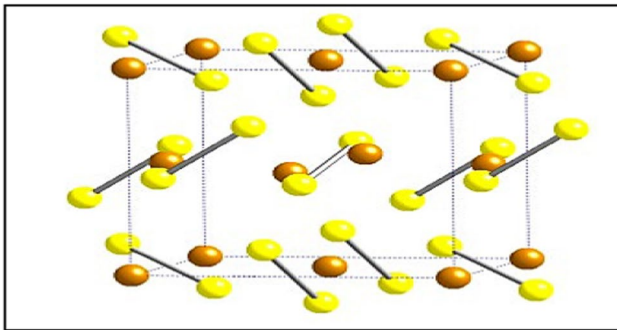


Fig. 11 Atomistic representation of a unit cell of pyrite. The brown spheres represent Fe and yellow spheres represent S. Reprinted with permission from Ref. 147. Copyright 2008, Springer Nature.

computations demonstrated that all of the examined compounds are excellent TE materials for *p*-type doping. Marcasite FeSe_2 performed better than any other material for *p*-type TE applications. The crystal symmetry was weaker than that of rock salt due to the sulfur dimers that occupy the anion sites along the $\langle 111 \rangle$ direction. A unit cell of pyrite contains four units of FeS_2 . The distorted octahedral field results from the coordination of each S atom to three Fe atoms and its dimer counterpart, as well as the coupling of each Fe atom to six S atoms,¹⁴⁷ as shown in Fig. 11.

The ideal form of iron pyrite, FeS_2 , is a 2D TMD with prospective uses in the chemical, optical, and electronics industries. Its small bandgap makes it perfect for ultrafast applications in the near-infrared spectrum.¹⁴⁸ FeS_2 is being considered as a potential component for TE and battery cathode applications.¹⁴⁹ Iron pyrite can be produced using a variety of vapor-phase and solution processing methods such as sulfurization of iron and iron oxide thin films, chemical vapor deposition, electrodeposition, spray pyrolysis, hydrothermal techniques, sputtering, hot injection, and electrochemical deposition.

FeS_2 exhibits higher thermal conductivity than CoS_2 and MS_2 .⁹² For its mineral compound and a single crystal, thermal conductivity values of $23 \text{ W m}^{-1} \text{ K}^{-1}$ and $45 \text{ W m}^{-1} \text{ K}^{-1}$, respectively, were reported. A new category of wide-bandgap *p*-type TE materials known as Cu_2MSnX_4 includes quaternary chalcogenides that resemble chalcopyrite and are doped with copper ($\text{M} = \text{Zn}, \text{Cd}; \text{X} = \text{S}, \text{Se}$).¹⁵⁰ The TE properties of undoped and doped FeS_2 are listed in Table V.

Due to the chemical instability by forming sulfuric acid and ferrous oxide when coming into contact with air and moisture, these materials are unsuitable as a TE material at high temperatures. In addition, their high conductivity impedes their application in this field. From the literature, it is also clear that pyrite as such has not shown any pronounced result as a TE material, but in the future, doping it with suitable impurities might bring this material into the actual area of TE applications. Therefore, it can be concluded that this branch of chalcogenide materials is still open for further exploration.

Table V TE properties of undoped and highly doped FeS_2 samples¹⁴⁹

Sample	Electrical conductivity (S m^{-1})	Seebeck coefficient ($\mu\text{V K}^{-1}$)	Thermal conductivity ($\text{W m}^{-1} \text{ K}^{-1}$)	ZT (300 K)
Undoped FeS_2 (<i>p</i> -type, 16 nm)	3.1	73	1.2	4.1×10^{-4}
5% Co-doped FeS_2 (<i>n</i> -type)	19.5	-53	2.3	7.0×10^{-4}
4% Se-doped FeS_2 (<i>p</i> -type)	10.1	63	1.7	8.0×10^{-4}

Tri- and Tetra-Chalcogenides

The transition metal tri-chalcogenides are a low-dimensional family of materials sharing similar distinctive physical properties. They have layered and chain-like characteristics in their crystal structure. Trigonal MX_6 prismatic columns form the framework of the structure. The monoclinic crystal structure is seen in the semiconductive ZrSe_3 compounds. The strong chalcogen–chalcogen bonds in the prisms, which preserve pairs of electrons per unit cell, are mostly responsible for the nonmetallic character of the crystal. Niobium and tantalum are two low-dimensional materials that are good examples of transition metal tri-chalcogenides. The electrical properties of these compounds are controlled primarily by metal pairing in chains and chalcogen pairing around metal atoms. A new set of halogenide transition metal tetra-chalcogenides with the general formula $(\text{MX}_4)_n\text{Y}$, where M is Nb or Ta, X is S or Se, Y is Cl, Br, or I, and n is 2, 3, or 4, were produced by heating the components in enclosed silica tubes at temperatures ranging from 500°C to 600°C. The TE properties of some of the tri- and tetra-TMCs are shown in Table VI.

Transition metal tetra-selenides (MSe_4) were examined by Gressier et al.¹⁵⁵ Recent research has led to the synthesis of novel transition metal tetra-chalcogenides $(\text{MX}_4)_n\text{Y}$ (M = Nb, Ta; X = S, Se; Y = halogen) in relation to low-dimensional phenomena such as the Peierls distortion and the sliding charge density wave (CDW). Each MX_4 chain contains an atom of a metal, M, sandwiched between two nearly rectangular X4 units.¹⁵⁶ Chianelli et al.¹⁵⁷ discovered that *n*-butyl-lithium typically produces a ternary phase of the form Li_3MX_3 when it reacts with transition metal tri-chalcogenides.¹⁵⁷ ZrSe_3 -type or TiS_3 -type are two extremely similar monoclinic structures that can be seen in either or both of the crystalline structures of transition metal tri-chalcogenides in bulk form. Figure 12 shows the TiS_3 crystal structure.

Anisotropic TE properties are thought to be significant in bulk, multilayer, and ML MX_3 materials. ZrS_3 has a greater PF ($S^2\sigma$) along the *x*-direction, but travels more slowly along the *y*-direction. According to the DFT investigations

of ZrSe_3 MLs, solid anisotropy of the electric transport characteristics might result from corrugated conduction levels.¹⁵⁵ Transition metal tri-chalcogenides are extraordinary two-dimensional materials that stand out from other materials due to their inherent electronic, optical, electrical, magnetic, and superconducting properties as well as their ability to transport CDWs.¹⁵⁹ While tremendous progress has been made, issues such as achieving high TE performance over a wide temperature range and improving the stability and dependability of TMC-based devices remain to be addressed before the branch can be brought into mainstream applications. However, continuous research and development of tri- and tetra-transition-metal chalcogenides shows potential for developing the TE technology and tackling global energy concerns.

Thermoelectric Applications of the Main-Group Chalcogenides

PbTe , GeTe , Bi_2Se_3 , Sb_2Te_3 , AgSbTe_2 , and $\text{Ge}_2\text{Sb}_2\text{Te}_5$ are a few of the main-group chalcogenides.^{160,161} These materials and their compounds have unique physical properties and are used in phase-transition materials, TE materials, and topological insulators. The inclusion of the main group of metals and the composition and structure of these materials have a significant impact on their characteristics. For chalcogen atoms and group 13/14 metals, tetrahedral coordination geometry is the most desirable coordination mode. Binary intermediate phases (In_2S_3 , In_2Se_3 , GeS , SnSe , and SnS) are frequently produced as reaction by-products. However, because of their low solubility in common solvents, metal and chalcogen ions may precipitate, impeding the formation of complex frameworks by the reaction process. The solvo-(hydro)thermal technique, high-temperature solid-state processes, solution synthesis, and others have all been used to create crystalline chalcogenides.¹⁶²

Metal monochalcogenides have the chemical formula MX , which comprises group IV metals such as Si, Ge, and Sn, and chalcogens such as S and Se. GeS possesses a direct bandgap between 1.58 eV and 1.61 eV, whereas SnS , SnSe ,

Table VI Thermoelectric properties of some of the tri- and tetra-transition metal chalcogenide systems

Sample	Method	Thermal conductivity ($\text{W m}^{-1} \text{K}^{-1}$)	<i>ZT</i>	Temperature	References
$\text{Na}_{0.05}\text{Cu}_9\text{S}_5$ nano-powders	BM + SPS	–	–	773	151
$\text{Ag}_2\text{ZnGeS}_4$	DFT	–	2.5	600	152
$\text{Ag}_2\text{PbGeS}_4$	DFT	–	2.5–3	600	
$\text{Cu}_2\text{CoSnSe}_4$	DFT	0.7	0.75	773	153
$\text{BaCu}_2\text{GeS}_4$	DFT	–	1.01	100	154

SPS spark plasma sintering, DFT density functional theory, BM ball milling

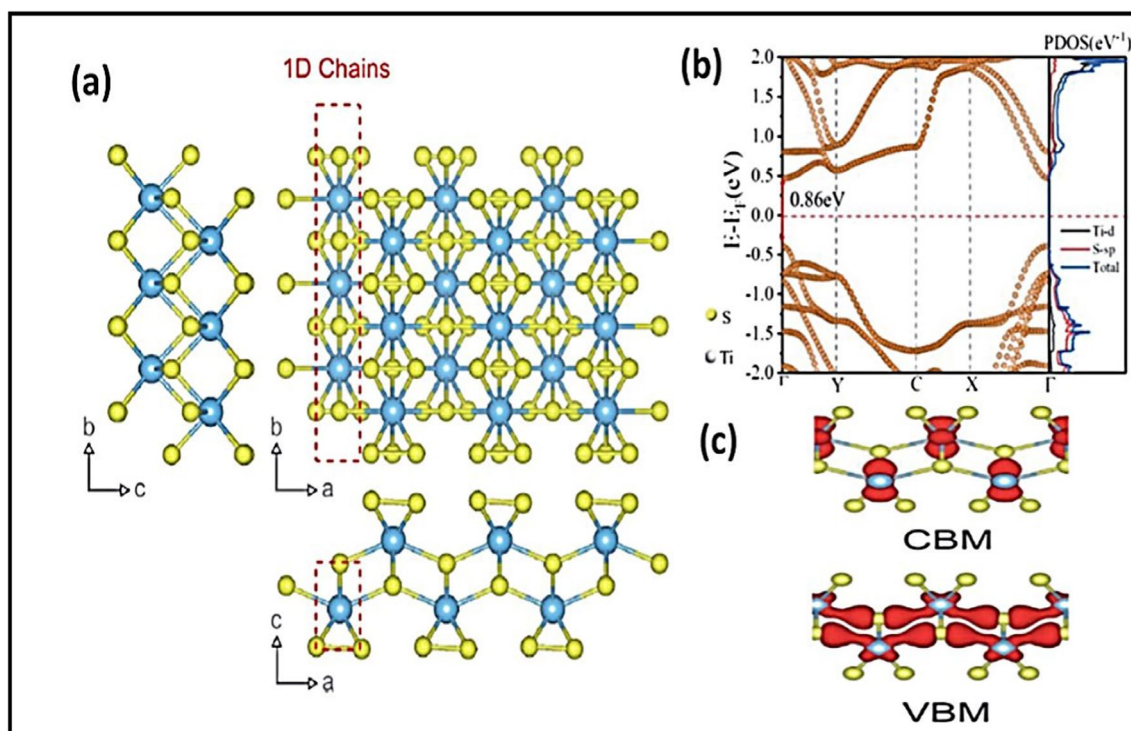


Fig. 12 (a) The crystal structure of anisotropic TiS_3 showing the bond lengths between titanium and sulfur along the b - and a -axis, with the shorter bonds along the b -axis. (b) Calculated electronic energy band structure along the symmetry directions of the Brillouin zone (G–Y–

C–X–G) and the projected density of states (PDOS) of the optimized structure of ML TiS_3 . The direct bandgap E_g of ML TiS_3 is indicated by the red arrows. Reprinted from Ref. 158, under Creative Commons license CC BY Copyright 2020, Royal Society of Chemistry.

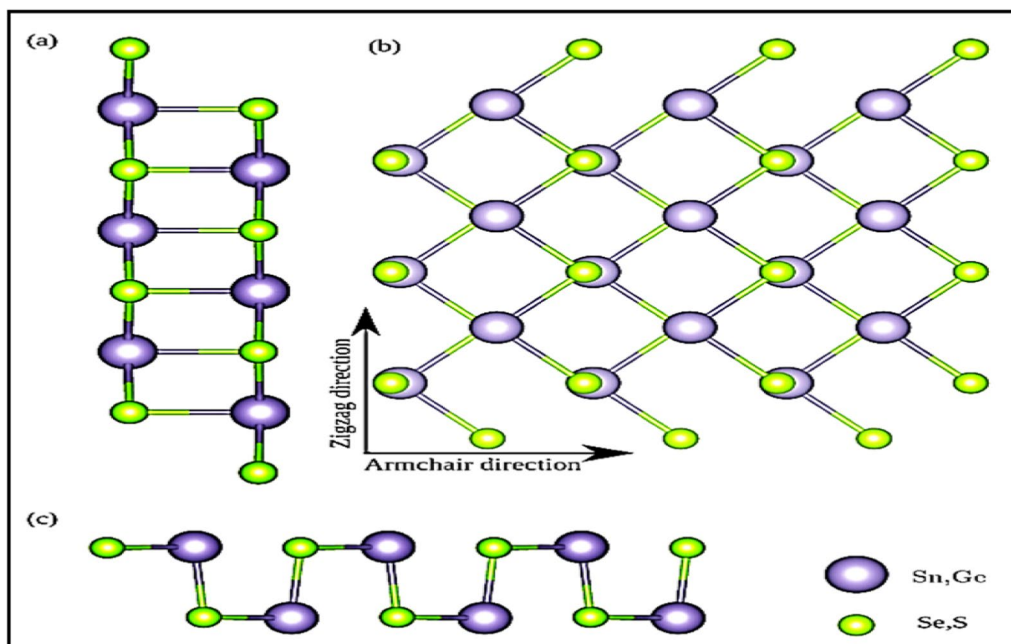


Fig. 13 Crystal structure of the 2D metal monochalcogenides SnSe, SnS, GeSe, and GeS. (a) Side view perpendicular to the zigzag direction, (b) top view, (c) side view perpendicular to the armchair direction. Reprinted from Ref. 163, under Creative Commons license CC BY.

Table VII Calculated lattice parameters and bandgaps of SnSe, SnS, GeSe, and GeS¹⁶³

Composition	Lattice parameter (Å)		Bandgap (eV)	
	Monolayer		Monolayer	Bulk
	<i>a</i>	<i>b</i>	GGA	GGA
SnSe	4.46	4.29	0.99	0.65
SnS	4.31	4.07	1.42	0.86
GeSe	4.41	3.99	1.16	0.83
GeS	4.48	3.70	1.71	1.18

GGA generalized gradient approximation

and GeSe have near-infrared (< 1.45 eV) indirect bandgaps. By the alternation of metal and chalcogen atoms along the zigzag (*y*) and armchair (*x*) planes, a puckered or wavy layer structure is created (Fig. 13).

Despite possessing a finite bandgap (as shown in Table VII), monochalcogenides exfoliated into atomically thin layers have attracted increasing interest because of their competitive characteristics compared to graphene. GeSe is a IV-VI *p*-type semiconductor with a layered crystal structure and a narrow bandgap of 1.08 eV.¹⁶⁴ The structural transitions between the phases lead to significant changes in the electrical characteristics of the material.^{165–167} Low-dimensional semiconducting materials with applications in the emerging microelectronics field have mainly focused on bandgap and high carrier mobility.^{168,169}

Monochalcogenides have significant *ZT* values at room temperature, with β -SnSe exhibiting a *ZT* ~ 2.06 at 300 K.¹²⁸ Since the TE properties of a material greatly depend on the structure of the crystal, Hu et al.¹⁶⁹ examined the energy and TE characteristics of four distinct SnSe (β , γ , δ , and ϵ) ML phases combined with α -SnSe using the ab initio DFT approach. Figure 14 presents the *ZT* values of SnSe MLs with different phases at 300 K. Using the semiclassical Boltzmann theory, the TE transport characteristics and coefficients were extracted from the electronic structure. Due to its nontoxic, earth-abundant, and chemically stable nature, SnSe exhibits the highest TE performance among the different TE materials and has potential uses in TE applications. Based on calculations of the TE characteristics at different doping levels, and because of its poor lattice thermal conductivity (Table VIII), β -SnSe exhibits the highest *ZT*.¹⁶⁷ For SnSe, *ZT* = 2.63 and 2.46; for SnS, *ZT* = 1.75 and 1.88; for GeSe, *ZT* = 1.99 and 1.73; and for GeS, *ZT* = 1.85 and 1.29 along the armchair and zigzag directions, respectively. Wubienh et al.¹⁷⁰ examined the effect of Ge doping on SnSe, and found that (Sn_{1-x}Ge_x)Se is a promising alternative for highly efficient TE materials. Further reducing the dimensionality can improve the efficiency of TE materials.¹⁶⁹

It is observed that two-dimensional materials have higher Seebeck coefficients than bulk structures, with GeS having the highest value, at 2810 $\mu\text{V K}^{-1}$ at ambient temperature. GeSe single crystals produced using several transport agents, such as physical vapor transport and chemical vapor transport using I_2 and NH_4Cl , were investigated by Solanki et al.¹⁷¹ for TE PF studies. According to their data analysis, GeSe is an effective TE material. GeTe, PbTe, and related materials showed low thermal conductivity, strong stability, and high *ZT* values in the moderate-temperature range of 300–900 K. Further improving their TE performance is possible by doping, making composites, building micro/nanostructures, and recrystallization of these materials. According to Hodges et al.,¹⁷² the new $\text{Pb}_{0.98-x}\text{Na}_{0.02-x}\text{HgSe}$ system has outperformed all other *p*-type PbSe systems to date and exhibited a PF value of 2000 $\text{W m}^{-1} \text{K}^{-2}$ at 950 K, setting a record-high *ZT* of 1.7. Increasing the PF is often far more challenging with top TE materials than reducing heat conductivity.¹⁷² The *ZT* values of some of the monochalcogenides are shown in Fig. 15 and listed in Table IX.

Recently, 2D main-group metal chalcogenides such as GeS, SnSe₂, and GaTe have attracted considerable attention. These layered semiconducting materials have excellent room-temperature stability, a low effective mass, and a programmable bandgap. According to theory, nanostructuring can enhance the *ZT* beyond the value in the bulk due to a decrease in κ , caused by increased phonon scattering at the edges of the nanostructure,²⁶ and the increase in *S* and σ caused by quantum confinement. The investigation of a new technique for synthesizing nanostructures of bismuth telluride and related alloys is currently in progress.¹⁸² The highest known *ZT* in bulk form is found in Bi₂Te₃-based TE materials.^{183–186} The crystal structures of Bi₂Te₃ and Bi₂Se₃ are formed by the quintuple stalk sequences of Te–Bi–Te and Se–Bi–Se. The bonds between Bi, Te, and Se are polar covalent bonds, whereas Se⁽¹⁾–Se⁽¹⁾ and Te⁽¹⁾–Te⁽¹⁾ with weak vdW bonding rise to an easy cleavage along *c* basal planes.^{187–189} With a bandgap of 1.3 eV, bismuth sulfide, or Bi₂S₃ (of a stibnite structure), offers significant potential in TE cooling. Their solid solutions are semiconductors, such as Bi₂Se₃, Bi₂Te₃, and Sb₂Te₃, which are well-known TE materials (Fig. 16).

With the right doping, both *n*- and *p*-type materials can be created. Electrochemical deposition in porous alumina templates can be used to produce aligned Bi₂Te₃ nanorods. However, they are usually polycrystalline and have poor charge carrier mobility. Figure 16 illustrates the improvement in *ZT* values for *n*- and *p*-type bismuth chalcogenide materials with different doping conditions. Liu et al.¹⁹⁰ investigated various Bi₂Te₃-Bi₂Se₃-Bi₂S₃ systems and demonstrated a maximum *ZT* of 0.8 at 300°C for Bi₂Te₂S₁ and at 500°C for Bi₂Se₁S₂ (Fig. 17). These findings indicate that

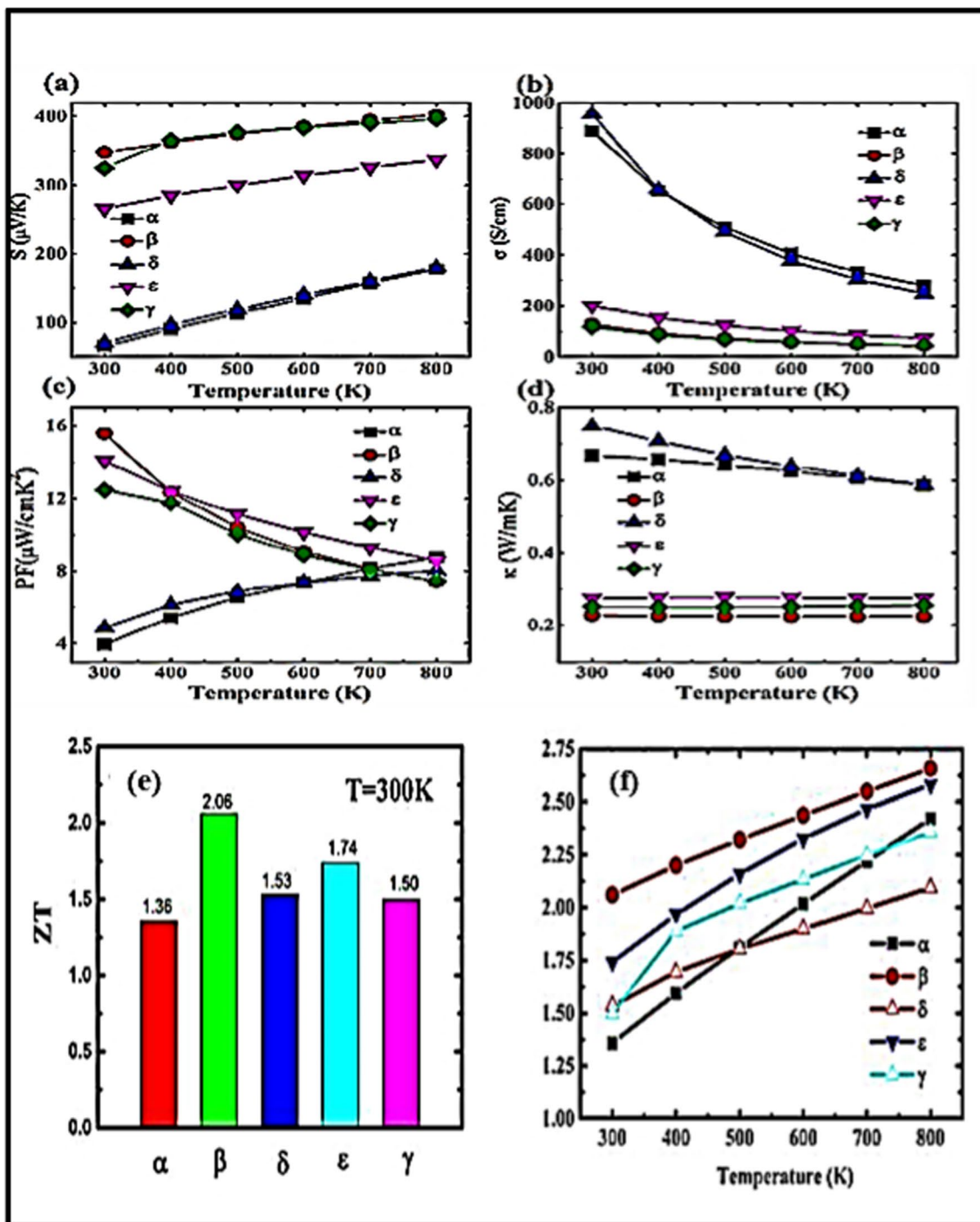


Fig. 14 (a) Seebeck coefficient, (b) electrical conductivity, (c) power factor, (d) total thermal conductivity, and (e) ZT values for five monolayer SnSe phases at a temperature of 300 K; (f) ZT values of

α -SnSe, β -SnSe, γ -SnSe, δ -SnSe, and ϵ -SnSe as a function of temperature from 300 K to 800 K. Reprinted with permission from Ref. 169. Copyright 2017, Royal Society of Chemistry.

these materials are appropriate for use in power generation at medium temperatures.

Hao et al.¹⁹³ reported 1.4 and 1.2 as the highest possible ZT values between 100°C and 300°C, respectively, for p -type Bi_2Te_3 materials with suppressed intrinsic excitation,

and reported increased conversion efficiency of 6% under 217 K temperature gradient when incorporated in a TE module. Kim et al.¹⁹⁴ performed band engineering on Bi_2Te_3 and Sb_2Te_3 , reporting a considerable increase in the density-of-state effective mass and carrier concentration while retaining

mobility. This technique resulted in a high ZT value of 1.05 at 300 K for $(\text{Bi}_{0.25}\text{Sb}_{0.75})_2\text{Te}_3$, indicating promising TE performance among the main-group chalcogenide materials (see Table X).

Zhu et al.¹⁹⁵ studied defect engineering in V2VI3 semiconductors, focusing on the effect of intrinsic point defects in improving the TE performance of these semiconductor

Table VIII Minimum lattice thermal conductivity, κ_{min} ($\text{W m}^{-1} \text{K}^{-1}$), and minimum and maximum ZT values (ZT_{min} and ZT_{max} , respectively) at 300/800 K for α -SnSe, β -SnSe, γ -SnSe, δ -SnSe, and ϵ -SnSe¹⁶⁹

Phases	κ_{min} ($\text{W m}^{-1} \text{K}^{-1}$)	ZT_{min}	ZT_{max}
α	0.175	1.362	2.420
β	0.156	2.061	2.658
δ	0.219	1.532	2.095
ϵ	0.162	1.743	2.582
γ	0.184	1.498	2.358

materials. Their findings highlight the potential for defect management to revitalize semiconductor materials used in TE applications. By employing microstructure engineering, Pan et al.¹⁹⁶ demonstrated that it was possible to reduce the lattice thermal conductivity (κ_{L}), which also increased the TE ZT . By controlling the development of dislocations and clean grain boundaries, the microstructure modification created a porous platelet-like network. The ZT value of 1.2 for this porous material was higher than that of the completely dense $(\text{BiSb})_2\text{Te}_3$ alloys that were prepared using hot-pressed and zone-melted ingots. $\text{Bi}_{0.5}\text{Sb}_{1.5}\text{Te}_3$ and $\text{Bi}_{0.3}\text{Sb}_{1.7}\text{Te}_3$ segmented legs with a high ZT above 1.0 may have device efficiency of up to 9% over the entire temperature range of 323–523 K. According to Luo et al.,¹⁹⁷ n-type SnSe_2 nanoplates with electron doping exhibit encouraging temperature-dependent TE performance, with a maximum ZT of 0.63 for 1.5 at.% Cl-doped $\text{SnSe}_{1.95}$ at 673 K, which is significantly greater than the ZT of 0.08 for pure SnSe_2 .¹⁹⁷

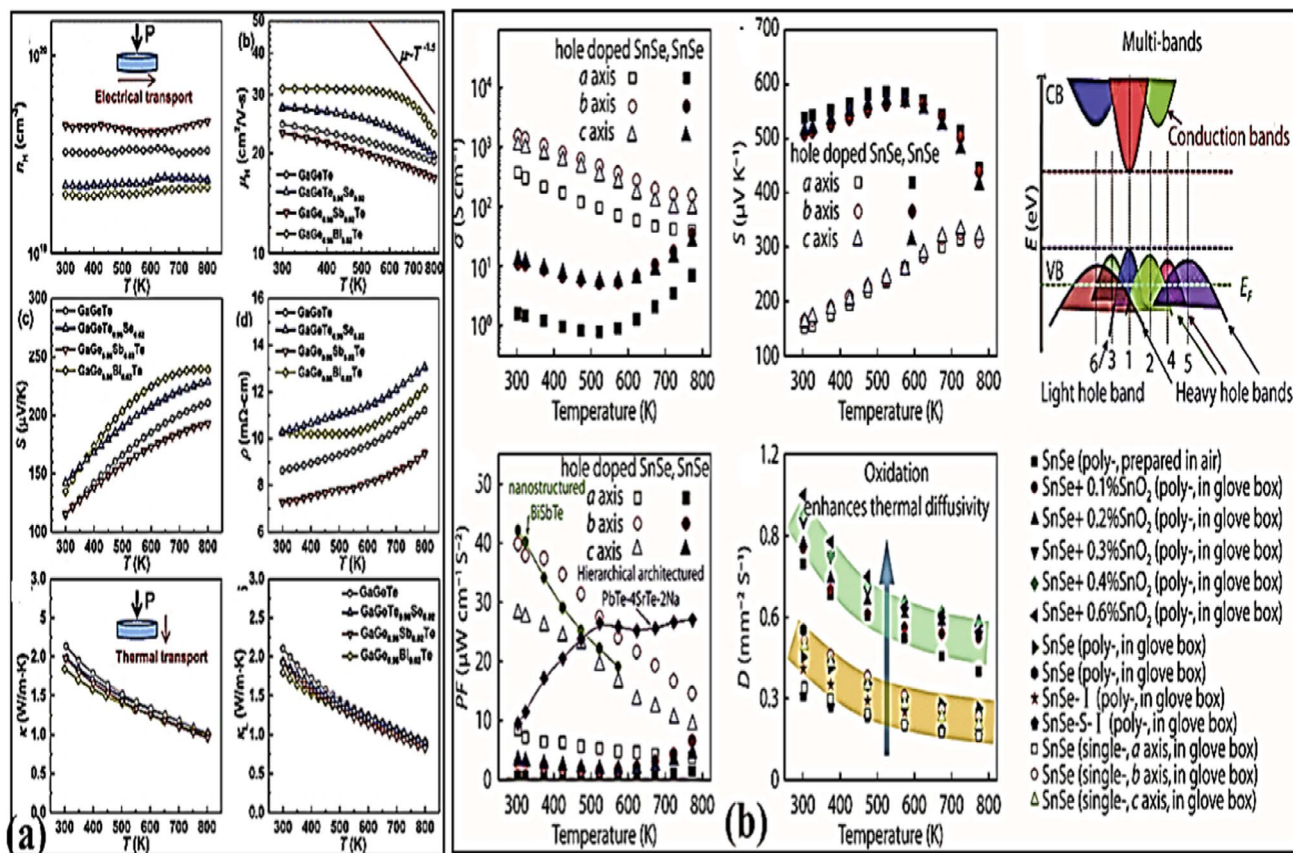


Fig. 15 (a) Temperature-dependent Hall carrier concentration, Hall mobility, Seebeck coefficient, resistivity, total thermal conductivity, and lattice thermal conductivity for pristine and doped GaGeTe hot-pressed materials; Reprinted with permission from Ref. 173. Copyright 2024, American Chemical Society. (b) Temperature-dependent electrical conductivity and Seebeck coefficient of undoped SnSe and hole-doped SnSe along the a , b , and c directions, schematic representation

of multivalent bands of SnSe, comparison of power factor of undoped SnSe crystal, hole-doped SnSe crystal, $\text{Bi}_{2-x}\text{Sb}_x$, and PbTe alloyed with 4 mol.% SrTe and doped with 2 mol.% Na, thermal diffusivity of polycrystalline SnSe with and without SnO_2 as a function of temperature. Reprinted with permission from Ref. 174. Copyright 2023, CC BY 4.0.

Table IX *ZT* values of some monochalcogenide materials^{128,168,173,175–181}

Material	Methods	Type	Temperature (K)	<i>ZT</i>
SnS _{0.91} Se _{0.09}	Temperature gradient method	–	873	1.6
SnSe–2SnTe	The modified Bridgman method	P	793	2.1
Sn _{0.97} Re _{0.03} Se _{0.93} Cl _{0.02}	Solid-state reaction and SPS	N	798	1.5
Sn _{1-x} Se (Sn vacancy level of 0.3%)	Improved horizontal Bridgman method	P	793	1.24
Sn _{0.95} Se	Hydrothermal method	P	873	2.1
SnSe with multiple nanopores	Simple solvothermal method	P	823	1.7
SnSe _{0.9} Br _{0.1}	Melting and HP	N	773	1.3
0.25 vol.% CNTs-SnSe	Cryogenic grinding and SPS	P	773	0.96
SnSe crystals	–	N	773	2.8
Sn _{1-x} Ag _x Se	DFT	–	0–1000	0.53
Sn _{1-x} Au _x Se	DFT	–	0–1000	0.68
<i>Cmcm</i> -phase SnSe	–	–	923	4.33
K _{0.01} Sn _{0.99} Se	Mechanical alloying and SPS	–	773	1.1
5% Bi ₂ Te ₃ doped-Ge _{0.87} Pb _{0.13} Te	Vacuum-melting and annealing + SPS process	–	775	2.1
Ge _{0.85} Mg _{0.05} Sb _{0.1} Te	Melting, annealing, and SPS	–	300–800	1.2
Ge _{0.86} Mn _{0.10} Sb _{0.04} Te	Melting, quenching, and annealing process combined with SPS	–	400–800	1.09
Ge _{0.94} Sb _{0.06} Te	MS-SPS	P	700	1.56
Ge _{0.81} Mn _{0.15} Bi _{0.04} Te	BM + HP	–	300–773	1.5
Ge _{0.85} (Pb _{0.9} Yb _{0.1}) _{0.15} Te	Conventional melting and SPS techniques	–	723	1.4
Ag-doped SnS	Mechanical alloying followed by spark plasma sintering	–	873	0.6
Hole-doped GeSe	–	–	300–800	0.8–2.5
SnSe	Solvothermal synthesized powders	–	> 773	0.6
GeS/phosphorene 2D heterostructures	First-principles study	–	300	2.53
GaGeTe	High-temperature melting	–	800	0.4
Ge _{0.96-x} Mn _x Bi _{0.04} Te	BM + HP	–	773	1.5
Ge _{0.94} Sb _{0.06} Te	MS + SPS	–	700	1.56
Ge _{0.89} Cu _{0.06} Sb _{0.08} Te	Traditional melting, annealing, and SPS	–	750	> 2.0
(Mg,Sb)-co-doped polycrystalline GeTe	Melting, annealing, and SPS	–	800	1.84
Na _{0.03} Eu _{0.03} Sn _{0.02} Pb _{0.92} Te	Lattice strain and band convergence	–	873	2.6
HgY ₂ S ₄	DFT	–	300	0.72
HgY ₂ Se ₄	DFT	–	300	0.75
Ge _{0.86} Mn _{0.10} Sb _{0.04} Te	Melting, quenching, and annealing	–	823	1.61
Pb _{0.953} Na _{0.040} Ge _{0.007} Te	Melting, grinding, and SPS	–	805	1.9
Sn _{0.82} Ag _{0.08} Pb _{0.1} Se	Mechanical alloying + SPS	–	800	1.33
Pb _{1.02} Se-0.2%Cu	Dual interstitial doping	N	773	1.3
Ge _{0.93} Pb _{0.04} Bi _{0.03} Te	DFT + doping	–	670	2.14
Sn _{0.96} Bi _{0.02} Mg _{0.02} Te	Solvothermal	–	584	0.21
Sn _{0.92} Mn _{0.11} Te	HPHT	–	773	1.1

SPS spark plasma sintering, DFT density functional theory, HP hydraulic press, BM ball milling, MS melt spin, HPHT high pressure high temperature

Hegde et al.^{198,199} showed a reduction in the electrical resistivity of (Bi_{0.96}In_{0.04})₂Se_{2.7}Te_{0.3}, which resulted in an increased PF of 1900 μW m⁻¹K⁻² with *ZT* = 0.28. Similarly, the authors reported tin-doped bismuth telluride with a *ZT* of 0.27 using a melt-growth technique. Zhu

et al.²⁰⁰ emphasized the importance of synthesis methods as well as materials in their study. Several growth approaches, including defect optimization, nanostructuring, and band engineering, resulted in high-*ZT* TE materials, with some reaching a value of 2. Nanostructuring,

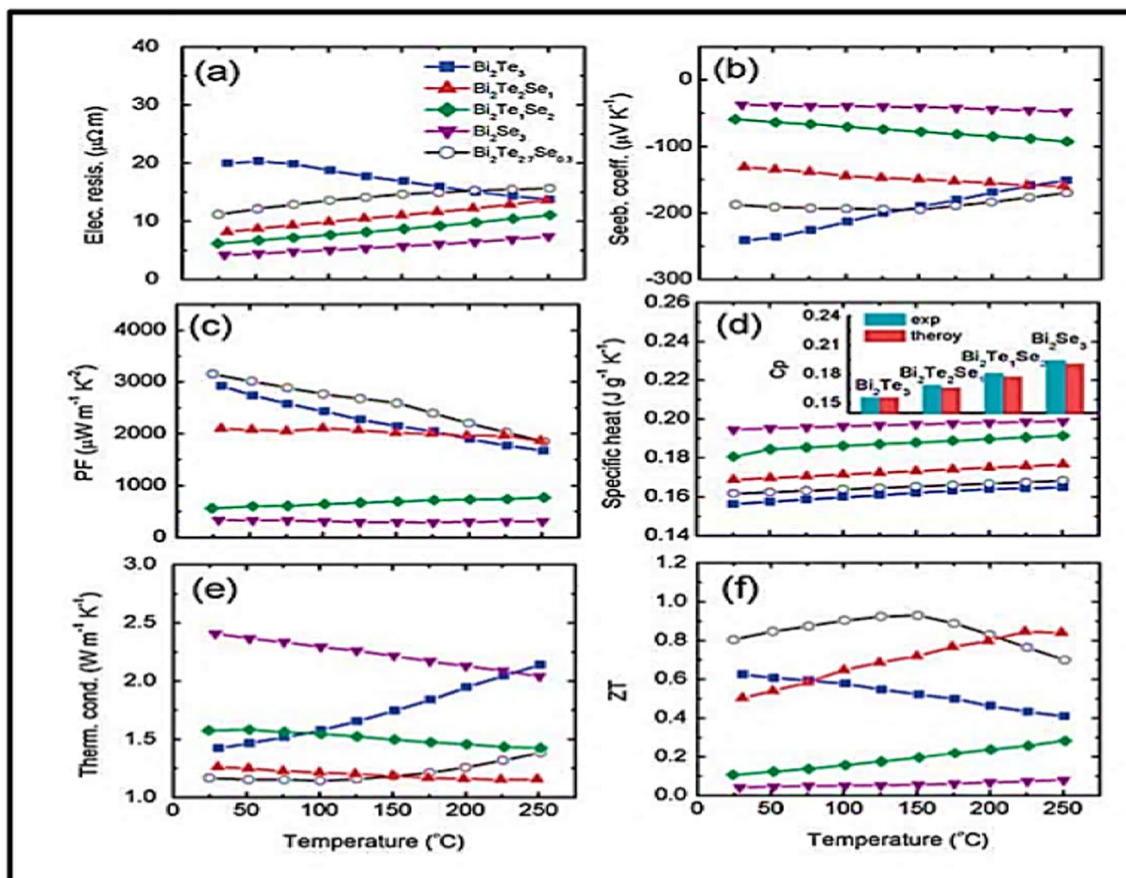


Fig. 16 Temperature-dependent TE properties of the Bi_2Te_3 - Bi_2Se_3 system: (a) electrical resistivity, (b) Seebeck coefficient, (c) PF, (d) specific heat, (e) thermal conductivity, and (f) figure of merit (ZT). The inset in (d) shows a comparison of the specific heat at room tem-

perature between the experimentally measured and theoretically calculated values. Reprinted with permission from Ref. 190. Copyright 2013, Royal Society of Chemistry.

by lowering the phonon mean free path, has the potential to improve the TE performance of the material.²⁰¹ MBE is frequently used to produce nanostructures of 2D layers on a solid material such as silicon.^{202–204} The ZT values of the main-group chalcogenide TE materials are listed in Table X.

Progress, Challenges, and Outlook

In this work, we have carefully reviewed the most recent progress in chalcogenide-based TE materials. The crystal structure, their basic properties, and the effect of doping and modification of the dimensionality on the TE properties of chalcogenide materials have been summarized in this article. The efficiency of the materials based on their TE properties and their efficiency in device applications were described through this review. Different synthesis methods for preparing these materials were also discussed. The review reveals that the solution-based method of

chemical synthesis outperforms chemical vapor deposition, and MBE has several advantages, including affordability, low energy use, and ease of scaling. Of crucial significance is the precise control of the reaction parameters such as temperature, concentration of catalysts, and dispersants, which enable chemical synthesis to more easily regulate the size, form, and composition of the 2D materials. Two-dimensional-type TMDs have often been produced using aqueous solution-based hydrothermal synthesis.^{211–213} The morphology and structure of the 2D materials can be affected by their hydrothermal synthesis, thus providing a new method for modifying their carrier mobility and concentration and making TMDs a great alternative for TE applications. Random porous structures are created by partially densifying a material to offer a distribution of pores throughout the structure. Although it is simple to create random porous structures, their impacts are limited by the lack of morphological control.¹⁹³ Small impurity additions made during the bottom-up manufacturing of semiconductor TE materials can

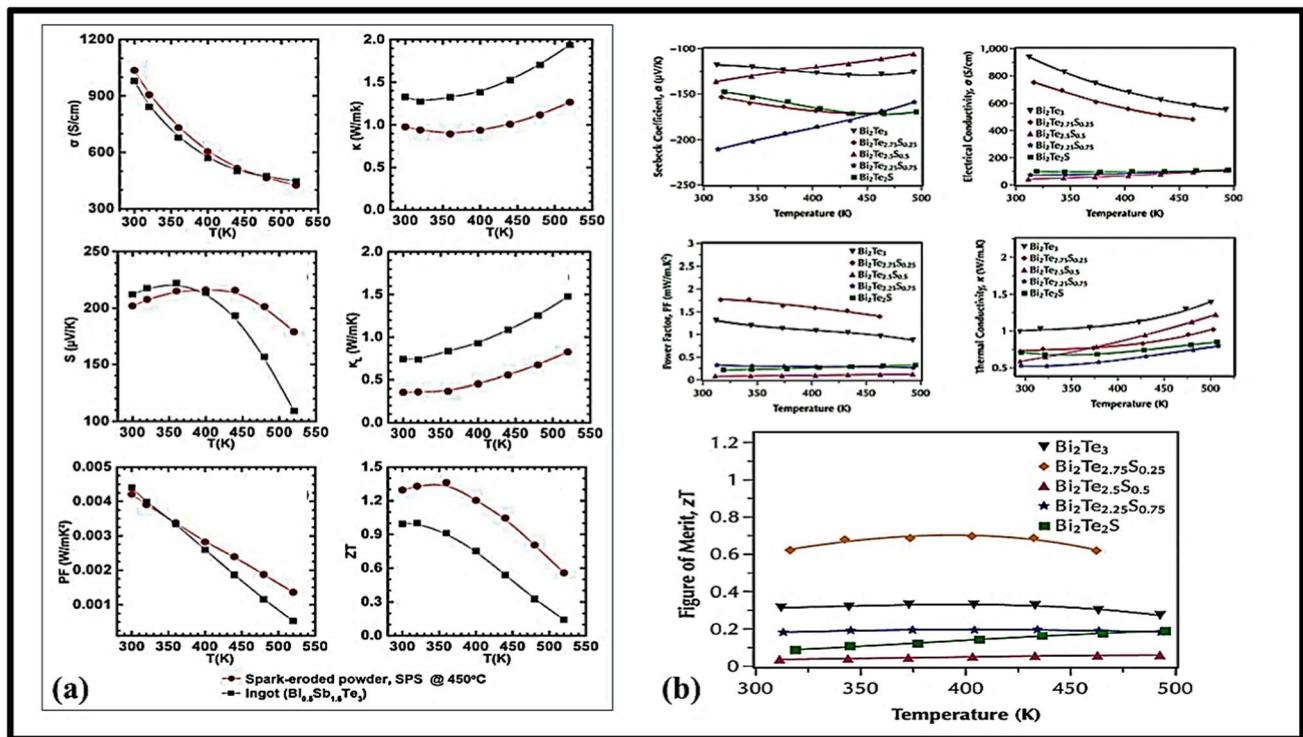


Fig. 17 (a) Temperature-dependent TE properties of Sb-doped Bi_2Te_3 . Reprinted with permission from Ref. 191. Copyright 2023, CC BY 4.0, Elsevier. (b) Temperature-dependent Seebeck coefficient,

electrical conductivity, power factor, total thermal conductivity, and figure of merit of $\text{Bi}_2\text{Te}_{3-x}\text{S}_x$ between 300 K and 500 K. Reprinted from Ref. 192, under Creative Commons license CC BY.

adjust the mobility and/or carrier concentration and also induce point defects and modify the microstructures.^{214,215} To obtain the optimal results, defect-engineering or stoichiometric control (typically 10^{19} cm^{-3}) can be used to alter the carrier concentration during synthesis, and this frequently requires further extrinsic doping.²⁰⁰ Although a large number of materials are classified under the main-group chalcogenides, there are still many less-explored materials that are not being synthesized or have received little attention. Among these are $\text{Bi}_2\text{O}_2\text{Se}$,²¹⁶ SnSb_2Te_4 ,²¹⁷ and their related compounds, which despite having a considerable Seebeck coefficient, due to their poor electrical properties are still in a stage of infancy and require further attention to enter the main branch of study.

Conclusion and Future Outlook

TE materials present possibilities for the creation of smart sensor devices, energy harvesting, thermopower wave sources, woodstoves, diesel power plants, and automobiles.

In addition, the use of TE chalcogenide-based material with high figures of merit is favored in TE device applications. Through techniques such as doping, energy band engineering, and artificial micro-nanostructure processing, material properties including electrical conductivity, thermal conductivity, and Seebeck coefficient of the materials are altered to enhance their ZT value. This review has revealed that Bi_2Te_3 nanowires showed the highest ZT of 2.5 at 350 K and can be considered a highly efficient material for device formation at room temperature or in the temperature range of 10–400 K, whereas the first-principles calculation predicts the best performance in the mid- and high-temperature range with the ZT of approximately 4.1 and 4.33 at 750 K and 923 K, respectively, for $Cmcm$ -phase SnSe nanotubes. Al- and Li-doped Cu_2Se are the preferred TE candidates, with ZT values of approximately 2.14 and 2.66 at 973 K and 1039 K, respectively. Hence, tuning the parameters of these candidates will be the most efficient method, with good conversion efficiency that can result in the best-fit materials for future applications.

However, the majority of mid- or high-temperature materials, such as Pb, As, Be, and Cd, are costly and contain toxic chemicals, making them unsuitable for use in actual applications. The development of effective TE materials has been hampered by numerous restrictions. The reproducibility of

Table X *ZT* values of the main-group chalcogenide TE materials 175,205–210

Materials	Methods	Type of material	Temperature (K)	<i>ZT</i> value
Bi ₂ Te ₃ bulk	Liquid-state manipulation	N	475	0.66
(Bi _{0.98} In _{0.02}) ₂ Te _{2.7} Se _{0.3}	Solid-state reaction techniques	N	350	0.6
Cu _{0.87} Bi ₂ Te _{2.69}	Disproportionation redox reaction	N	415	0.67
Bi ₂ Te ₃ -CaSiO ₃	Physical blending and calcination	P	373	0.72
Bi _{1.95} Ge _{0.05} Te ₃	Solid melt	N	300	0.95
Bi _{0.4} Sb _{1.6} Te ₃ -8 mol.% FeTe ₂	High-temperature solid-state reaction	P	396	1.52
Bi _{0.5} Sb _{1.5} Te ₃	Bottom-up solution synthesis	P	370	1.59
2.0 mol.%-Au-nanodot/BT-nanotube	Bottom-up synthesis	N	480	0.95
Y _{0.25} Bi _{1.75} Te ₃	Hydrothermal method	P	410	1.23
Bi _{2.0} Te _{2.7} Se _{0.3}	Arc plasma torch	N	300	1.47
Bi ₂ Te ₃ nanowires	–	–	350	2.5
Bi ₂ Te ₃ /Sb ₂ Te ₃ superlattice	–	P	300	2.4
BiI ₃ -doped Sb ₂ Te ₃ (GeTe) ₁₇	Melting, annealing, and SPS	–	723	2.2
Ge ₉ Sb ₂ Te _{12-x} (<i>x</i> =0, 0.03, 0.06, 0.09, 0.12, 0.15)	Vacuum-melting + annealing + SPS	–	775	2.1
Na _{0.02} Pb _{0.98-x} Mg _x Te _{0.8} Se _{0.2}	Melting and SPS	–	800	2.0
3 mol.% Bi ₂ Te ₃ -doped Ge _{0.87} Pb _{0.13} Te	–	–	773	1.9
PbTe/PbTe _{0.75} Se _{0.25}	Evaporation process	–	425	1.75
Ge _{1-2x} Te(CuSb) _x (<i>x</i> =0.025, 0.05, 0.075, 0.10) composites	Solid-phase reaction	–	773	1.62
Ge _{0.75} Pb _{0.25} Te _{0.5} Se _{0.5}	Melting, solutioning, and quenching route + SPS	–	673	1.6
(Pb _{0.9} Yb _{0.1} Te) _{0.15} (GeTe) _{0.85}	Melting, annealing, and HP	–	750	1.4
SnS ₂	Nanoflakes	–	300	0.13
SnSe ₂	Nanosheet pellets	–	673	0.63
Bi ₂ Se ₃ thin films	Thermal evaporation	–	300	–
Bi ₂ Te ₃ CNT + silica aerogel films	Doping + sintering	–	400	1.1 (<i>p</i> -type) 1.01 (<i>n</i> -type)
Bi ₂ Te _{2.75} S _{0.25}	Direct reaction	–	400	0.7
SnSe ₂	DFT calculation	–	673	0.56
Bi ₂ Te _{2.7} Se _{0.3}	Zone melting	–	360	1.16
Sb ₂ Te ₃ -SWCNT + Sb ₂ Te ₃ -electrodeposition	Redox reaction technique	–	300	–
Bi _{0.55} Sb _{1.45} Te ₃ + 2.5 wt.% Bi	Mechanical alloying + BM + HP	P	360	1.45
Bi _{2-y} La _y Te _{2.7-3} Se _{0.3}	BM + SPS	N	300–400	0.87
Bi _{1.94} Sb _{0.06} Te ₃	HP	–	430	1.97
Sn _{0.3} Bi ₂ Se ₃	Melt growth	–	835	0.2
Bi ₂ S ₂ Se + wt.1% BiI ₃	Solid-state method + SPS	–	673	0.65

SPS spark plasma sintering, DFT density functional theory, HP hydraulic press, BM ball milling

the *ZT* value constitutes the major obstacle. Concerns about reliability and efficiency also need to be considered. It takes a combination of theoretical direction, sharp chemical intuition, synthetic chemistry competence, materials processing, and good measurement skills to find promising novel materials. Resolving these restrictions could eventually result in the commercialization of a clean electricity generator or Peltier device for refrigeration applications. In addition,

standardization will also be required in the fabrication of TE materials to guarantee the quality and success of commercialization. It is anticipated that TE materials will gain more application potential in the future.

Acknowledgments The authors are thankful for the financial support provided by Dr. T. M. A Pai fellowship from the Manipal Academy of Higher Education. The authors wish to express their gratitude to fellow researchers Ms. Mariot Panjikanan and Mr. Vipin Cyriac for their

invaluable contributions. Their meticulous efforts in review corrections and insightful technical advice have been instrumental in enhancing the quality of this work. One of the authors, GSH, express their gratitude to REVA University for their collaborative support in writing the manuscript.

Author Contributions Ashwatha Narayana Prabhu: Idea for the review article, Supervision, Validation, Correction. Suchitra Puthran: Literature survey and analysis, writing the first draft. Ganesh Hegde: Idea for writing techniques, Correction.

Funding Open access funding provided by Manipal Academy of Higher Education, Manipal.

Conflict of interest The authors have no conflict to declare.

Open Access This article is licensed under a Creative Commons Attribution 4.0 International License, which permits use, sharing, adaptation, distribution and reproduction in any medium or format, as long as you give appropriate credit to the original author(s) and the source, provide a link to the Creative Commons licence, and indicate if changes were made. The images or other third party material in this article are included in the article's Creative Commons licence, unless indicated otherwise in a credit line to the material. If material is not included in the article's Creative Commons licence and your intended use is not permitted by statutory regulation or exceeds the permitted use, you will need to obtain permission directly from the copyright holder. To view a copy of this licence, visit <http://creativecommons.org/licenses/by/4.0/>.

References

1. A. Bahrami, G. Schierning, and K. Nielsch, Waste recycling in thermoelectric materials. *Adv. Energy Mater.* 10(19), 1904159 (2020). <https://doi.org/10.1002/aenm.201904159>.
2. J.R. Sootsman, D.Y. Chung, and M.G. Kanatzidis, New and old concepts in thermoelectric materials. *Angew. Chem. Int. Ed.* 48(46), 8616 (2009). <https://doi.org/10.1002/anie.200900598>.
3. C. Jangonda, K. Patil, A. Kinikar, R. Bhokare, and M.D. Gavali, Review of various application of thermoelectric module. *IJIR-SET* 5(3), 3393 (2016).
4. M. Elgendi, A.E. Kabeel, and F.A. Essa, Improving the solar still productivity using thermoelectric materials: a review. *Alex. Eng. J.* 65, 963 (2023). <https://doi.org/10.1016/j.aej.2022.10.011>.
5. L. Huang, Y. Zheng, L. Xing, and B. Hou, Recent progress of thermoelectric applications for cooling/heating, power generation, heat flux sensor and potential prospect of their integrated applications. *Therm. Sci. Eng. Prog.* 45, 102064 (2023). <https://doi.org/10.1016/j.tsep.2023.102064>.
6. N. Jaziri, N. Gutzeit, H. Bartsch, A. Boughamoura, J. Müller, and F. Tounsi, LTCC-based Y-type thermoelectric generator with an improved heat flow guide for automotive waste heat recovery. *Sustain. Energy Fuels* 6, 2330 (2022). <https://doi.org/10.1039/D2SE00048B>.
7. K.-W. Du and C.-I. Wu, An innovative tubular thermoelectric generator (TTEG) for enhanced waste heat recovery in industrial and automotive applications. *Appl. Sci.* 14(2), 685 (2024).
8. Y. Wang, Y. Shi, D. Mei, and Z. Chen, Wearable thermoelectric generator to harvest body heat for powering a miniaturized accelerometer. *Appl. Energy* 215, 690 (2018). <https://doi.org/10.1016/j.apenergy.2018.02.062>.
9. N. Swarnkar, Review of thermoelectric materials and its properties with applications. *JETIR* 6(5), 131 (2019).
10. D. Suryawanshi, V. Pokale, N. Pokharkar, A. Walgude, and P. Patunkar, A review of performance analysis & potential applications of thermoelectric refrigeration system. *IJRSI* III(III), 29 (2016).
11. D.M. Rowe, *CRC handbook of thermoelectrics* (Boca Raton: CRC Press, 1995).
12. J. He and T.M. Tritt, Advances in thermoelectric materials research: looking back and moving forward. *Science (New York, N.Y.)* 357(6358), eaak9997 (2017). <https://doi.org/10.1126/science.aak9997>.
13. J. Yang, H.L. Yip, and A.K.Y. Jen, Rational design of advanced thermoelectric materials. *Adv. Energy Mater.* 3(5), 549 (2013). <https://doi.org/10.1002/aenm.201200514>.
14. D. Enescu and E.O. Virjoghe, A review on thermoelectric cooling parameters and performance. *Renew. Sustain. Energy Rev.* 38, 903 (2014). <https://doi.org/10.1016/j.rser.2014.07.045>.
15. G. Tan, L.D. Zhao, and M.G. Kanatzidis, Rationally designing high-performance bulk thermoelectric materials. *Chem. Rev.* 116(19), 12123 (2016). <https://doi.org/10.1021/acs.chemrev.6b00255>.
16. M.N. Hasan, H. Wahid, N. Nayan, and M.S. Mohamed Ali, Inorganic thermoelectric materials: a review. *Int. J. Energy Res.* 44, 6170 (2020). <https://doi.org/10.1002/er.5313>.
17. B.C. Sales, D. Mandrus, B.C. Chakoumakos, V. Keppens, and J.R. Thompson, Filled skutterudite antimonides: electron crystals and phonon glasses. *Phys. Rev. B* 56, 15081 (1997). <https://doi.org/10.1103/PhysRevB.56.15081>.
18. Z.G. Mei, J. Yang, Y.Z. Pei, W. Zhang, L.D. Chen, and J. Yang, Alkali-metal-filled CoSb₃ skutterudites as thermoelectric materials: theoretical study. *Phys. Rev. B* 77, 045202 (2008). <https://doi.org/10.1103/PhysRevB.77.045202>.
19. N.P. Blake, S. Lattner, J.D. Bryan, G.D. Stucky, and H. Metiu, Band structures and thermoelectric properties of the clathrates Ba₈Ga₁₆Ge₃₀, Sr₈Ga₁₆Ge₃₀, Ba₈Ga₁₆Si₃₀, and Ba₈In₁₆Sn₃₀. *J. Chem. Phys.* 115, 8060 (2001). <https://doi.org/10.1063/1.1397324>.
20. J.J. Gutiérrez Moreno, J. Cao, M. Fronzi, and M.H.N. Assadi, A review of recent progress in thermoelectric materials through computational methods. *Mater. Renew. Sustain. Energy* 9, 16 (2020). <https://doi.org/10.1007/s40243-020-00175-5>.
21. H. Zhu, C. Xiao, and Y. Xie, Design of highly efficient thermoelectric materials: tailoring reciprocal-space properties by real-space modification. *Adv. Mater.* 30, 1802000 (2018). <https://doi.org/10.1002/adma.201802000>.
22. G.S. Nolas, J.L. Cohn, G.A. Slack, and S.B. Schujman, Semiconducting Ge clathrates: promising candidates for thermoelectric applications. *Appl. Phys. Lett.* 73, 178 (1998). <https://doi.org/10.1063/1.121747>.
23. A. Bientien, V. Pacheco, S. Paschen, Y. Grin, and F. Steglich, Transport properties of composition tuned α - and β -Eu₈Ga_{16-x}Ge_{30+x}. *Phys. Rev. B* 71, 165206 (2005). <https://doi.org/10.1103/PhysRevB.71.165206>.
24. N.O. Nenuwe and E. Omugbe, Electronic properties of half-Heusler compounds XCrSb (X = Fe, Ru, Os): potential applications as spintronics and high-performance thermoelectric materials. *Curr. Appl. Phys.* 49, 70 (2023). <https://doi.org/10.1016/j.cap.2023.02.013>.
25. R. Bueno Villoro, D. Zavanelli, C. Jung, D.A. Mattlat, R. Hatami Naderloo, N. Pérez, K. Nielsch, G.J. Snyder, C. Scheu, R. He, and S. Zhang, Grain boundary phases in NbFeSb half-Heusler alloys: a new avenue to tune transport properties of thermoelectric materials. *Adv. Energy Mater.* 13, 2204321 (2023). <https://doi.org/10.1002/aenm.202204321>.
26. Q. Shen, L. Chen, T. Goto, T. Hirai, J. Yang, G.P. Meisner, and C. Uher, Effects of partial substitution of Ni by Pd on the thermoelectric properties of ZrNiSn-based half-Heusler compounds. *Appl. Phys. Lett.* 79, 4165 (2001). <https://doi.org/10.1063/1.1425459>.

27. T. Caillat, J.-P. Fleurial, and A. Borshchevsky, Preparation and thermoelectric properties of semiconducting Zn_4Sb_3 . *J. Phys. Chem. Solids* 58(7), 1119 (1997). [https://doi.org/10.1016/S0022-3697\(96\)00228-4](https://doi.org/10.1016/S0022-3697(96)00228-4).
28. I.R. Fisher, S.L. Bud'ko, C. Song, P.C. Canfield, T.C. Ozawa, and S.M. Kauzlarich, $\text{Yb}_{14}\text{ZnSb}_{11}$: charge balance in zintl compounds as a route to intermediate Yb valence. *Phys. Rev. Lett.* 85, 1120 (2000). <https://doi.org/10.1103/PhysRevLett.85.1120>.
29. S.M. Kauzlarich, S.R. Brown, and G. Jeffrey Snyder, Zintl phases for thermoelectric devices. *Dalton Trans.* 21, 2099 (2007). <https://doi.org/10.1039/B702266B>.
30. Y.S. Wudil, M.A. Gondal, M.A. Almessiere, and A.Q. Alsayoud, The multi-dimensional approach to synergistically improve the performance of inorganic thermoelectric materials: a critical review. *Arab. J. Chem.* 14(4), 103103 (2021). <https://doi.org/10.1016/j.arabjc.2021.103103>.
31. T. Hendricks, T. Caillat, and T. Mori, Keynote review of latest advances in thermoelectric generation materials, devices, and technologies 2022. *Energies* 15(19), 7307 (2022). <https://doi.org/10.3390/en15197307>.
32. J. He, K. Li, L. Jia, Y. Zhu, H. Zhang, and J. Linghu, Advances in the applications of thermoelectric generators. *Appl. Therm. Eng.* 236(Part D), 21813 (2024). <https://doi.org/10.1016/j.applthermaleng.2023.121813>.
33. E. Muchuweni and E.T. Mombeshora, Recent advances in thermoelectric performance by incorporating graphene-based materials for energy harvesting. *Renew. Energy Focus* 45, 40 (2023).
34. M. Saha, O. Tregenza, J. Twelftree, and C. Hulston, A review of thermoelectric generators for waste heat recovery in marine applications. *Sustain. Energy Technol. Assess.* 59, 103394 (2023). <https://doi.org/10.1016/j.seta.2023.103394>.
35. C. Han, Q. Sun, Z. Li, and S.X. Dou, Thermoelectric enhancement of different kinds of metal chalcogenides. *Adv. Energy Mater.* 6, 1600498 (2016). <https://doi.org/10.1002/aenm.20160498>.
36. T. Plirdpring, K. Kurosaki, A. Kosuga, T. Day, S. Firdosy, V. Ravi, G.J. Snyder, A. Harnwungmoung, T. Sugahara, Y. Ohishi, H. Muta, and S. Yamanaka, Chalcopyrite CuGaTe_2 : a high-efficiency bulk thermoelectric material. *Adv. Mater.* 24, 3622 (2012). <https://doi.org/10.1002/adma.201200732>.
37. M. Kumagai, K. Kurosaki, Y. Ohishi, H. Muta, and S. Yamanaka, Effect of ball-milling conditions on thermoelectric properties of polycrystalline CuGaTe_2 . *Mater. Trans.* 55, 1215 (2014). <https://doi.org/10.2320/matertrans.E-M2014821>.
38. X.B. Zhao, X.H. Ji, Y.H. Zhang, T.J. Zhu, J.P. Tu, and X.B. Zhang, Bismuth telluride nanotubes and the effects on the thermoelectric properties of nanotube-containing nanocomposites. *Appl. Phys. Lett.* 86(6), 062111 (2005). <https://doi.org/10.1063/1.1863440>.
39. C. Lin, W. Cheng, Z. Guo, G. Chai, and H. Zhang, Exceptional thermoelectric performance of a "star-like" SnSe nanotube with ultra-low thermal conductivity and a high power factor. *Phys. Chem. Chem. Phys.* 19, 23247 (2017). <https://doi.org/10.1039/C7CP04508E>.
40. G.C. Tewari, T.S. Tripathi, H. Yamauchi, and M. Karppinen, Thermoelectric properties of layered antiferromagnetic CuCrSe_2 . *Mater. Chem. Phys.* 145, 156 (2014). <https://doi.org/10.1016/j.matchemphys.2014.01.053>.
41. F. Gascoin, A. Maignan, Order-disorder transition in AgCrSe_2 : a new route to efficient thermoelectrics. *Chem. Mater.* 23, 2510 (2011). <https://doi.org/10.1021/cm200581k>.
42. S. Bhattacharya, A. Bohra, R. Basu, R. Bhatt, S. Ahmad, K.N. Meshram, A.K. Debnath, A. Singh, S.K. Sarkar, M. Navneethan, Y. Hayakawa, D.K. Aswal, and S.K. Gupta, High thermoelectric performance of $(\text{AgCrSe}_2)_{0.5}(\text{CuCrSe}_2)_{0.5}$ nano-composites having all-scale natural hierarchical architectures. *J. Mater. Chem. A Mater.* 2, 17122 (2014). <https://doi.org/10.1039/C4TA04056B>.
43. S.N. Zhang, T.J. Zhu, S.H. Yang, C. Yu, and X.B. Zhao, Improved thermoelectric properties of AgSbTe_2 based compounds with nanoscale Ag_2Te in situ precipitates. *J. Alloys Compd.* 499, 215 (2010). <https://doi.org/10.1016/j.jallcom.2010.03.170>.
44. D. Byeon, R. Sobota, K. Delime-Codrin, S. Choi, K. Hirata, M. Adachi, M. Kiyama, T. Matsuura, Y. Yamamoto, M. Matsunami, and T. Takeuchi, Discovery of colossal seebeck effect in metallic Cu_2Se . *Nat. Commun.* 10, 72 (2019). <https://doi.org/10.1038/s41467-018-07877-5>.
45. L. Pan, D. Bérardan, and N. Dragoë, High thermoelectric properties of N-type AgBiSe_2 . *J. Am. Chem. Soc.* 135, 4914 (2013). <https://doi.org/10.1021/ja312474n>.
46. O. Yamashita and H. Odahara, Influence of annealing on the distribution of thermoelectric figure of merit in bismuth-telluride ingots. *J. Mater. Sci.* 41, 323 (2006). <https://doi.org/10.1007/s10853-005-2209-z>.
47. B. Qin, D. Wang, W. He, Y. Zhang, H. Wu, S.J. Pennycook, and L.D. Zhao, Realizing high thermoelectric performance in p-type SnSe through crystal structure modification. *J. Am. Chem. Soc.* 141, 1141 (2019). <https://doi.org/10.1021/jacs.8b12450>.
48. W. Wei, C. Chang, T. Yang, J. Liu, H. Tang, J. Zhang, Y. Li, F. Xu, Z. Zhang, J.-F. Li, and G. Tang, Achieving high thermoelectric figure of merit in polycrystalline SnSe via introducing Sn vacancies. *J. Am. Chem. Soc.* 140, 499 (2018). <https://doi.org/10.1021/jacs.7b11875>.
49. Z.J. Chen, T. Shen, R.K. Nutor, S.D. Yang, H.F. Wu, and J.X. Si, Influence of local heterojunction on the thermoelectric properties of Mo-SnSe multilayer films deposited by magnetron sputtering. *J. Electron. Mater.* 48, 1153 (2019). <https://doi.org/10.1007/s11664-018-06849-1>.
50. B. Zhong, Y. Zhang, W. Li, Z. Chen, J. Cui, Y. Xie, Q. Hao, and Q. He, High superionic conduction arising from aligned large lamellae and large figure of merit in bulk $\text{Cu}_{1.94}\text{Al}_{0.02}\text{Se}$. *Appl. Phys. Lett.* 105, 123902 (2014). <https://doi.org/10.1063/1.4896520>.
51. A.S.M. Sayem, A. Lalbakhsh, K.P. Esselle, J.L. Buckley, B. O'Flynn, and R.B.V.B. Simorangkir, Flexible transparent antennas: advancements, challenges, and prospects. *IEEE Open J. Antennas Propag.* 3, 1109 (2022). <https://doi.org/10.1109/OJAP.2022.3206909>.
52. P. Wu and J.A. Ibers, Quaternary chalcogenides containing a rare earth and an alkali- or alkaline-earth metal. *J. Alloys Compd.* 229(1), 206 (1995). [https://doi.org/10.1016/0925-8388\(95\)01676-7](https://doi.org/10.1016/0925-8388(95)01676-7).
53. G. Zuo, Z. Li, E. Wang, and M. Kemerink, High seebeck coefficient and power factor in n-type organic thermoelectrics. *Adv. Electron. Mater.* 4, 1700501 (2018). <https://doi.org/10.1002/aelm.201700501>.
54. Y. Nonoguchi, M. Nakano, T. Murayama, H. Hagino, S. Hama, K. Miyazaki, R. Matsubara, M. Nakamura, and T. Kawai, Simple salt-coordinated n-type nanocarbon materials stable in air. *Adv. Funct. Mater.* 26, 3021 (2016). <https://doi.org/10.1002/adfm.201600179>.
55. B. Dörling, X. Rodríguez-Martínez, I. Álvarez-Corzo, J.S. Reparaz, and M. Campoy-Quiles, Soluble alkali-metal carbon nanotube salts for n-type thermoelectric composites with improved stability. *Appl. Phys. Lett.* 118, 213901 (2021). <https://doi.org/10.1063/5.0047338>.
56. M.A.K. Lodhi, P. Vijayaraghavan, and A. Daloglu, Simulation and analysis of time-dependent degradation behavior of AMTEC. *J. Power. Sources* 96(2), 343 (2001). [https://doi.org/10.1016/S0378-7753\(00\)00664-9](https://doi.org/10.1016/S0378-7753(00)00664-9).

57. S.D. Kim, H.T. Kim, D.W. Seo, S. Young Kim, M.S. Suh, and S.K. Woo, Novel Mo/TiN composites for an alkali metal thermal-to-electric converter (AMTEC) electrode. *Ceram. Int.* 40(9), 14247 (2014). <https://doi.org/10.1016/j.ceramint.2014.06.014>.
58. L. Zhu, L. Chen, H. Li, D. Li, N. Yang, X. Jiang, and S. Qiu, Performance analysis of alkali metal thermoelectric converter and segmented thermoelectric generator hybrid system based on a comprehensive model. *Appl. Therm. Eng.* 183(Part 1), 116206 (2021). <https://doi.org/10.1016/j.applthermaleng.2020.116206>.
59. K. Rajput and D.R. Roy, h-CaS and h-CaSe nanosheets in CaX (X = O, S, Se and Te) series: promising thermoelectric materials under DFT investigation. *Appl. Nanosci.* 9, 1845 (2019). <https://doi.org/10.1007/s13204-019-00997-4>.
60. M. Irfan, S. Azam, A. Dahshan, I. El Bakkali, and K. Nouneh, First-principles study of opto-electronic and thermoelectric properties of SrCdSnX₄ (X = S, Se, Te) alkali metal chalcogenides. *Comput. Condens. Matter* 30, e00625 (2022). <https://doi.org/10.1016/j.cocom.2021.e00625>.
61. N. Kapuria, B. Nan, T.E. Adegoke, U. Bangert, A. Cabot, S. Singh, and K.M. Ryan, Colloidal synthesis of multinary alkali-metal chalcogenides containing Bi and Sb: an emerging class of I-V-VI₂ nanocrystals with tunable composition and interesting properties. *Chem. Mater.* 35(12), 4810 (2023). <https://doi.org/10.1021/acs.chemmater.3c00673>.
62. H. Lin, G. Tan, J.N. Shan, S. Hao, L.M. Wu, N. Calta, C. Malliakas, S. Wang, C. Uher, C. Wolverton, and M.G. Kanatzidis, Concerted rattling in CsAg₅Te₃ leading to ultralow thermal conductivity and high thermoelectric performance. *Angew. Chem. Int. Ed.* 55(38), 11431 (2016). <https://doi.org/10.1002/anie.201605015>.
63. L. Li, L. Wang, X. Dong, Y. Jiang, J. Ding, and N. Yuan, New nanofibrous structured CsAg₅Te₃ exhibiting ultralow thermal conductivity and high figure of merit. *ACS Omega* 8(48), 46182 (2023). <https://doi.org/10.1021/acsomega.3c07284>.
64. Z. Abbas, K. Fatima, I. Gorczyca, S.H.A. Jaffery, A. Ali, M. Irfan, H.H. Raza, H. Algarni, S. Muhammad, H. Teisseyre, and S. Hussain, First-principles calculations to investigate electronic, optical, and thermoelectric properties of Na₂GeX₃ (X = S, Se, Te) for energy applications. *Mater. Sci. Semicond. Process.* 154, 107206 (2023). <https://doi.org/10.1016/j.mssp.2022.107206>.
65. G. Nazir, A.S. Alofi, A. Rehman, Q. Mahmood, M. mana AL-Anazy, R. Karmouch, M.F. Rahman, and E.S. Yousef, Rare earth based Mg-chalcogenides MgDy₂(S/Se)₄ as an emerging aspirant for spintronic and thermoelectric applications. *Mater. Sci. Semicond. Process.* 173, 108129 (2024). <https://doi.org/10.1016/j.mssp.2024.108129>.
66. A. Assoud, N. Soheilnia, and H. Kleinke, Thermoelectric properties of the new tellurides SrSc₂Te₄ and BaSc₂Te₄ in comparison to BaY₂Te₄. *Intermetallics* 15(3), 371 (2007). <https://doi.org/10.1016/j.intermet.2006.08.006>.
67. B. Gul, M.S. Khan, A.A. Lfseisi, and H. Ahmad, First-principles study of potassium-based novel chalcogenide materials for optoelectronic and thermoelectric devices. *Phys. Scr.* 98(11), 115927 (2023). <https://doi.org/10.1088/1402-4896/acfeaa>.
68. H. Lin, G. Tan, J.-N. Shen, S. Hao, L.-M. Wu, N. Calta, C. Malliakas, S. Wang, C. Uher, C. Wolverton, and M.G. Kanatzidis, Concerted rattling in CsAg₅Te₃ leading to ultralow thermal conductivity and high thermoelectric performance. *Angew. Chem. Int. Ed.* 55(38), 11431 (2016). <https://doi.org/10.1002/anie.201605015>.
69. W. Jaegermann and H. Tributsch, Interfacial properties of semi-conducting transition metal chalcogenides. *Prog. Surf. Sci.* 29(1–2), 1 (1988). [https://doi.org/10.1016/0079-6816\(88\)90015-9](https://doi.org/10.1016/0079-6816(88)90015-9).
70. J.A. Wilson and A.D. Yoffe, The transition metal dichalcogenides discussion and interpretation of the observed optical, electrical and structural properties. *Adv. Phys.* 18(73), 193 (1969). <https://doi.org/10.1080/00018736900101307>.
71. D. Yoo, M. Kim, S. Jeong, J. Han, and J. Cheon, Chemical synthetic strategy for single-layer transition-metal chalcogenides. *J. Am. Chem. Soc.* 136(42), 14670 (2014). <https://doi.org/10.1021/ja5079943>.
72. B. Balasubramaniam, N. Singh, P. Kar, A. Tyagi, J. Prakash, and R.K. Gupta, Engineering of transition metal dichalcogenide-based 2D nanomaterials through doping for environmental applications. *Mol. Syst. Des. Eng.* 4, 804 (2019). <https://doi.org/10.1039/C8ME00116B>.
73. A.K. Gautam, M. Faraz, and N. Khare, Enhanced thermoelectric properties of MoS₂ with the incorporation of reduced graphene oxide (RGO). *J. Alloys Compd.* 838, 155673 (2020). <https://doi.org/10.1016/j.jallcom.2020.155673>.
74. A. Pramitha and Y. Raviprakash, Recent developments and viable approaches for high-performance supercapacitors using transition metal-based electrode materials. *J. Energy Storage* 49, 104120 (2022). <https://doi.org/10.1016/j.est.2022.104120>.
75. D. Siegmund, N. Blanc, M. Smialkowski, K. Tschulik, and U.P. Apfel, Metal-rich chalcogenides for electrocatalytic hydrogen evolution: activity of electrodes and bulk materials. *ChemElectroChem* 7(7), 1514 (2020). <https://doi.org/10.1002/celec.201902125>.
76. S. Azam, S. Goumri-Said, S.A. Khan, and M.B. Kanoun, Electronic, optical and thermoelectric properties of new metal-rich homologous selenides with palladium–indium: density functional theory and Boltzmann transport model. *J. Phys. Chem. Solids* 138, 109229 (2020). <https://doi.org/10.1016/j.jpcs.2019.109229>.
77. P. Vaqueiro, Solvothermal synthesis and thermoelectric properties of new complex tellurides InnovTEG-INNOVATIVE LOW-COST THERMOELECTRICS FOR RENEWABLE SOLAR ENERGY APPLICATIONS view project leverhulme project: understanding ultralow thermal conduction in copper-containing sulfides view project solvothermal synthesis and thermoelectric properties of new complex tellurides, n.d.
78. T.K. Reynolds, J.G. Bales, and F.J. DiSalvo, Synthesis and properties of a new metal-rich nickel antimonide telluride or selenide: Ni_{7–Δ}SbX₂ (δ ≈ 1.3; X = Se or Te). *Chem. Mater.* 14(11), 4746 (2002). <https://doi.org/10.1021/cm020585r>.
79. H.F. Franzen, M.X. Umara, J.R. McCreary, and R.J. Thorn, XPS spectra of some transition metal and alkaline earth monochalcogenides. *J. Solid State Chem.* 18(4), 363 (1976). [https://doi.org/10.1016/0022-4596\(76\)90119-5](https://doi.org/10.1016/0022-4596(76)90119-5).
80. L. Meng, Y. Li, J. Wu, L. Zhao, and J. Zhong, A type of novel weyl semimetal candidate: layered transition metal monochalcogenides Mo₂XY (X, Y = S, Se, Te, X ≠ Y). *Nanoscale* 12, 4602 (2020). <https://doi.org/10.1039/C9NR09123H>.
81. K.H. Jin and F. Liu, 1D topological phases in transition-metal monochalcogenide nanowires. *Nanoscale* 12, 14661 (2020). <https://doi.org/10.1039/D0NR03529G>.
82. H.T. Chin, M. Hofmann, S.Y. Huang, S.F. Yao, J.J. Lee, C.C. Chen, C.C. Ting, and Y.P. Hsieh, Ultra-thin 2D transition metal monochalcogenide crystals by planarized reactions. *npj 2D Mater. Appl.* 5, 28 (2021). <https://doi.org/10.1038/s41699-021-00207-2>.
83. M. Nagata, S. Shukla, Y. Nakanishi, Z. Liu, Y.-C. Lin, T. Shiga, Y. Nakamura, T. Koyama, H. Kishida, T. Inoue, N. Kanda, S. Ohno, Y. Sakagawa, K. Suenaga, and H. Shinohara, Isolation of single-wired transition-metal monochalcogenides by carbon nanotubes. *Nano Lett.* 19(8), 4845 (2019). <https://doi.org/10.1021/acs.nanolett.8b05074>.
84. L. Meng, J. Wu, Y. Li, and J. Zhong, Dirac–Weyl semimetal phase in noncentrosymmetric transition metal monochalcogenides

- MoTe and WTe. *J. Mater. Chem. C* 7, 12151 (2019). <https://doi.org/10.1039/C9TC03339D>.
85. L. Gao, J.-T. Sun, J.-C. Lu, H. Li, K. Qian, S. Zhang, Y.-Y. Zhang, T. Qian, H. Ding, X. Lin, S.X. Du, and H.-J. Gao, Epitaxial growth of honeycomb monolayer CuSe with dirac nodal line fermions. *Adv. Mater.* 30, 1707055 (2018). <https://doi.org/10.1002/adma.201707055>.
 86. F.H. Sun, H. Li, J. Tan, L. Zhao, X. Wang, H. Hu, C. Wang, and T. Mori, Review of current ZT > 1 thermoelectric sulfides. *Materiomics* 10(1), 218 (2024).
 87. A. Basit, J. Xin, G. Murtaza, L. Wei, A. Hameed, W. Guoyu, and J.Y. Dai, Recent advances, challenges, and perspective of copper-based liquid-like thermoelectric chalcogenides: a review. *Eco-Mat.* 5(9), e12391 (2023). <https://doi.org/10.1002/eom2.12391>.
 88. S. Xiang, D. Zhang, Y. Liang, X. Ma, and X. Zhang, Enhancing the thermal stability of S/Se based thermoelectric materials using self-generated oxide films. *Ceram. Int.* 49(19), 31325 (2023). <https://doi.org/10.1016/j.ceramint.2023.07.080>.
 89. P. Qiu, X. Shi, and L. Chen, Cu-based thermoelectric materials. *Energy Storage Mater.* 3, 85 (2016). <https://doi.org/10.1016/j.ensm.2016.01.009>.
 90. Y. He, T. Zhang, X. Shi, S.H. Wei, and L. Chen, High thermoelectric performance in copper telluride. *NPG Asia Mater.* 7, e210 (2015). <https://doi.org/10.1038/am.2015.91>.
 91. H. Chen, H. Lin, Z.-X. Lin, J.-N. Shen, L. Chen, and L.-M. Wu, Superionic adjustment leading to weakly temperature-dependent ZT values in bulk thermoelectrics. *Inorg. Chem.* 54(3), 867 (2015). <https://doi.org/10.1021/ic502102e>.
 92. H. Liu, X. Shi, F. Xu, L. Zhang, W. Zhang, L. Chen, Q. Li, C. Uher, T. Day, and G. Snyder Jeffrey, Copper ion liquid-like thermoelectrics. *Nat. Mater.* 11, 422 (2012). <https://doi.org/10.1038/nmat3273>.
 93. R.S. Sankar, S. Anwar, and S. Anwar, Enhanced thermoelectric power factor in the Cu₂Se system by the incorporation of GO/MWCNT. *Physica B* 652, 414620 (2023). <https://doi.org/10.1016/j.physb.2022.414620>.
 94. A.K. Gautam and N. Khare, Enhanced thermoelectric figure of merit at near room temperature in N-type binary silver telluride nanoparticles. *J. Materiomics* 9(2), 310 (2023). <https://doi.org/10.1016/j.jmat.2022.10.003>.
 95. Y. He, T. Day, T. Zhang, H. Liu, X. Shi, L. Chen, and G.J. Snyder, High thermoelectric performance in non-toxic earth-abundant copper sulfide. *Adv. Mater.* 26, 3974 (2014). <https://doi.org/10.1002/adma.201400515>.
 96. D.S. Nkemeni, Z. Yang, S. Lou, G. Li, and S. Zhou, Achievement of extra-high thermoelectric performance in doped copper(I) sulfide. *J. Alloys Compd.* 878, 160128 (2021). <https://doi.org/10.1016/j.jallcom.2021.160128>.
 97. L.J. Zheng, B.P. Zhang, H.Z. Li, J. Pei, and J.B. Yu, Cu_xS superionic compounds: electronic structure and thermoelectric performance enhancement. *J. Alloys Compd.* 722, 17 (2017). <https://doi.org/10.1016/j.jallcom.2017.06.078>.
 98. H. Tang, H.-L. Zhuang, B. Cai, J. Dong, F.-H. Sun, and J.-F. Li, Enhancing the thermoelectric performance of Cu_{1.8}S by Sb/Sn co-doping and incorporating multiscale defects to scatter heat-carrying phonons. *J. Mater. Chem. C* 7, 4026 (2019). <https://doi.org/10.1039/C9TC01096C>.
 99. W. Di Liu, X.-L. Shi, H. Gao, R. Moshwan, S.-D. Xu, Y. Wang, L. Yang, Z.-G. Chen, and J. Zou, Kinetic condition driven phase and vacancy enhancing thermoelectric performance of low-cost and eco-friendly Cu_{2-x}S. *J. Mater. Chem. C* 7, 5366 (2019). <https://doi.org/10.1039/C9TC00819E>.
 100. X. Chen, H. Zhang, Y. Zhao, W.-D. Liu, W. Dai, T. Wu, X. Lu, C. Wu, W. Luo, Y. Fan, L. Wang, W. Jiang, Z.-G. Chen, and J. Yang, Carbon-encapsulated copper sulfide leading to enhanced thermoelectric properties. *ACS Appl. Mater. Interfaces* 11(25), 22457 (2019). <https://doi.org/10.1021/acsami.9b06212>.
 101. Y.X. Zhang, Y.-K. Zhu, J. Feng, and Z.-H. Ge, Precious metal nanoparticles dispersing toward highly enhanced mechanical and thermoelectric properties of copper sulfides. *J. Alloys Compd.* 892, 162035 (2022). <https://doi.org/10.1016/j.jallcom.2021.162035>.
 102. Q. Yang, C. Ming, P. Qiu, Z. Zhou, X. Qiu, Z. Gao, T. Deng, L. Chen, and X. Shi, Incommensurately modulated structure in AgCuSe-based thermoelectric materials for intriguing electrical, thermal, and mechanical properties. *Small* 19, 2300699 (2023). <https://doi.org/10.1002/sml.202300699>.
 103. T. Wang, K. Zhao, P. Qiu, Q. Song, L. Chen, and X. Shi, Aguilrite Ag₄SSe thermoelectric material: natural mineral with low lattice thermal conductivity. *ACS Appl. Mater. Interfaces* 11(13), 12632 (2019). <https://doi.org/10.1021/acsami.8b22741>.
 104. P. Jood and M. Ohta, Temperature-dependent structural variation and Cu substitution in thermoelectric silver selenide. *ACS Appl. Energy Mater.* 3(3), 2160 (2020). <https://doi.org/10.1021/acsaelm.9b02231>.
 105. B. Feng, Y. Cheng, C. Liu, J. Gao, G. Wu, X. Bai, R. Si, W. Li, Y. Guo, and L. Miao, Ag interstitial inhibition and phonon scattering at the ZnSe nano-precipitates to enhance the thermoelectric performance of Ag₂Se. *ACS Appl. Energy Mater.* 6, 2804 (2023). <https://doi.org/10.1021/acsaelm.2c03704>.
 106. Y. Lu, Y. Qiu, K. Cai, X. Li, M. Gao, C. Jiang, and J. He, Ultra-high performance PEDOT/Ag₂Se/CuAgSe composite film for wearable thermoelectric power generators. *Mater. Today Phys.* 14, 100223 (2020). <https://doi.org/10.1016/j.mtphys.2020.100223>.
 107. Q.X. Hu, W.-D. Liu, L. Zhang, W. Sun, H. Gao, X.-L. Shi, Y.-L. Yang, Q. Liu, and Z.-G. Chen, SWCNTs/Ag₂Se film with superior bending resistance and enhanced thermoelectric performance via in situ compositing. *Chem. Eng. J.* 457, 141024 (2023). <https://doi.org/10.1016/j.cej.2022.141024>.
 108. Y. Lei, R. Qi, M. Chen, H. Chen, C. Xing, F. Sui, L. Gu, W. He, Y. Zhang, T. Baba, T. Baba, H. Lin, T. Mori, K. Koumoto, Y. Lin, and Z. Zheng, Microstructurally tailored thin β-Ag₂Se films toward commercial flexible thermoelectrics. *Adv. Mater.* 34, 2104786 (2022). <https://doi.org/10.1002/adma.202104786>.
 109. Y. Yu, D. Yang, J. Li, M. Zhang, H. Luo, Q. Liang, H. Ye, Q. Zhang, X. Tang, and J. Wu, A flash vacuum-induced reaction in preparing high performance thermoelectric Cu₂S. *Adv. Funct. Mater.* 32, 2107284 (2022). <https://doi.org/10.1002/adfm.202107284>.
 110. D. Yang, X. Su, J. Li, H. Bai, S. Wang, Z. Li, H. Tang, K. Tang, T. Luo, Y. Yan, J. Wu, J. Yang, Q. Zhang, C. Uher, M.G. Kanatzidis, and X. Tang, Blocking ion migration stabilizes the high thermoelectric performance in Cu₂Se composites. *Adv. Mater.* 32(40), 2003730 (2020). <https://doi.org/10.1002/adma.202003730>.
 111. Z. Zhu, Y. Zhang, H. Song, and X.J. Li, High thermoelectric performance and low thermal conductivity in Cu_{2-x}NaxSe bulk materials with micro-pores. *Appl. Phys. A* 125, 572 (2019). <https://doi.org/10.1007/s00339-019-2870-8>.
 112. S. Kavirajan, J. Archana, S. Harish, M. Omprakash, M. Naveenath, S. Ponnusamy, C. Muthamizhchelvan, Y. Inatomi, M. Shimomura, and Y. Hayakawa, Enhanced seebeck coefficient and low thermal conductivity of Cu₂Se_xTe_{1-x} solid solutions via minority carrier blocking and interfacial effects. *J. Alloys Compd.* 835, 155188 (2020). <https://doi.org/10.1016/j.jallcom.2020.155188>.
 113. H. Ju, D. Park, M. Kim, and J. Kim, Copper telluride with manipulated carrier concentrations for high-performance solid-state thermoelectrics. *J. Mater. Sci. Technol.* 129, 190 (2022). <https://doi.org/10.1016/j.jmst.2022.05.004>.

114. S. Acharya, B.K. Yu, J. Hwang, J. Kim, and W. Kim, High thermoelectric performance of ZnO by coherent phonon scattering and optimized charge transport. *Adv. Funct. Mater.* 31(43), 2105008 (2021). <https://doi.org/10.1002/adfm.202105008>.
115. H. Huang, W. Li, C. Hu, and X. Fan, Promising novel thermoelectric materials: two-dimensional penta-like PtPX (X = S, Se, Te) nanosheets. *J. Mater. Chem. C Mater.* 11(28), 9449 (2023). <https://doi.org/10.1039/D3TC01160G>.
116. T.R. Wei, C.F. Wu, F. Li, and J.F. Li, Low-cost and environmentally benign selenides as promising thermoelectric materials. *J. Materiomics* 4(4), 304 (2018). <https://doi.org/10.1016/j.jmat.2018.07.001>.
117. T.R. Wei, P. Qiu, K. Zhao, X. Shi, and L. Chen, Ag₂Q-based (Q = S, Se, Te) silver chalcogenide thermoelectric materials. *Adv. Mater.* 35(1), 2110236 (2023). <https://doi.org/10.1002/adma.202110236>.
118. M. Ohtaki, T. Tsubota, K. Eguchi, and H. Arai, High-temperature thermoelectric properties of (Zn_{1-x}Al_x)O. *J. Appl. Phys.* 79, 1816 (1996). <https://doi.org/10.1063/1.360976>.
119. T. Tsubota, M. Ohtaki, K. Eguchi, and H. Arai, Thermoelectric properties of Al-doped ZnO as a promising oxide material for high-temperature thermoelectric conversion. *J. Mater. Chem.* 7, 85 (1997).
120. S. Wei, L. Yu, Z. Zhang, Z. Ji, S. Luo, J. Liang, W. Song, and S. Zheng, Enhancing the effective mass and covalent bond strength of Cu₃SbSe₄-based thermoelectric materials by Mn/Sn co-doping. *Mater. Today Phys.* 38, 101260 (2023). <https://doi.org/10.1016/j.mtphys.2023.101260>.
121. W. Tang, W. Qian, S. Jia, K. Li, Z. Zhou, J. Lan, Y.H. Lin, and X. Yang, BiCuSeO based thermoelectric materials: innovations and challenges. *Mater. Today Phys.* 35, 101104 (2023).
122. S. Wei, Z. Ji, W. Li, S. Zheng, Q. Wang, Z. Li, L. Yu, S. Luo, and W. Song, Enhanced thermoelectric properties of Cu₃SbSe₄-based materials by synergistic modulation of carrier concentration and phonon scattering. *J. Materiomics* 10(2), 339 (2024). <https://doi.org/10.1016/j.jmat.2023.06.005>.
123. Y. Liu, J. Zhi, W. Li, Q. Yang, L. Zhang, and Y. Zhang, Oxide materials for thermoelectric conversion. *Molecules* 28(15), 5894 (2023). <https://doi.org/10.3390/molecules28155894>.
124. L.C. Gomes and A. Carvalho, Phosphorene analogues: iso-electronic two-dimensional group-IV monochalcogenides with orthorhombic structure. *Phys. Rev. B* 92, 085406 (2015). <https://doi.org/10.1103/PhysRevB.92.085406>.
125. A.M. Ibrahim and D.A. Thompson, Thermoelectric properties of BiSb alloys. *Mater. Chem. Phys.* 12(1), 29 (1985).
126. G. Shi and E. Kioupakis, Anisotropic spin transport and strong visible-light absorbance in few-layer SnSe and GeSe. *Nano Lett.* 15(10), 6926 (2015). <https://doi.org/10.1021/acs.nanolett.5b02861>.
127. T. Heine, Transition metal chalcogenides: ultrathin inorganic materials with tunable electronic properties. *Acc. Chem. Res.* 48(1), 65 (2015). <https://doi.org/10.1021/ar500277z>.
128. Z. Hu, Y. Ding, X. Hu, W. Zhou, X. Yu, and S. Zhang, Recent progress in 2D group IV–IV monochalcogenides: synthesis, properties, and applications. *Nanotechnology* 30(25), 252001 (2019). <https://doi.org/10.1088/1361-6528/ab07d9>.
129. Z. Tabaie and A. Omidvar, Human body heat-driven thermoelectric generators as a sustainable power supply for wearable electronic devices: recent advances, challenges, and future perspectives. *Heliyon* 9(4), e14707 (2023). <https://doi.org/10.1016/j.heliyon.2023.e14707>.
130. J. Ji, X. Song, J. Liu, Z. Yan, C. Huo, S. Zhang, M. Su, L. Liao, W. Wang, Z. Ni, Y. Hao, and H. Zeng, Two-dimensional antimonene single crystals grown by Van der Waals epitaxy. *Nat. Commun.* 7, 13352 (2016). <https://doi.org/10.1038/ncomms13352>.
131. I. Pallecchi, N. Manca, B. Patil, L. Pellegrino, and D. Marré, Review on thermoelectric properties of transition metal dichalcogenides. *Nano Futures* 4(3), 032008 (2020). <https://doi.org/10.1088/2399-1984/ab92f4>.
132. A. Kumari, A. Nag, and J. Kumar, Strain engineering and thermoelectric performance of janus monolayers of titanium dichalcogenides: a DFT study. *Comput. Mater. Sci.* 218, 111925 (2023). <https://doi.org/10.1016/j.commatsci.2022.111925>.
133. Z.R. Parekh, M.P. Deshpande, S.V. Bhatt, H.R. Bhoi, R.M. Kannaujiya, Y.V. Joshi, S.J. Pandya, and S.H. Chaki, Bridgman grown CuSbS₂ single crystal and its application as photodetector and potential thermoelectric material. *J. Alloys Compd.* 968, 171738 (2023). <https://doi.org/10.1016/j.jallcom.2023.171738>.
134. D. Zhang, M. Xie, D. Safanama, K. Saglik, X.Y. Tan, S.F.D. Solco, J. Cao, C.K.I. Tan, H. Liu, S. Wang, Q. Zhu, W.H.D. Fam, Q. Yan, J. Wu, and A. Suwardi, Sb alloying for engineering high-thermoelectric ZT of CuGaTe₂. *Adv. Energy Sustain. Res.* 4, 2300069 (2023). <https://doi.org/10.1002/aesr.202300069>.
135. Z. Bai, Y. Ji, and B. Qin, Microstructure and thermoelectric properties of marcasite-type compounds XTe₂ (X = Fe Co, Ni) prepared by solid-state reaction. *J. Mater. Sci. Mater. Electron.* 34, 461 (2023).
136. L. Zhang, B. Qin, C. Sun, Y. Ji, and D. Zhao, Effect of synthesis factors on microstructure and thermoelectric properties of FeTe₂ prepared by solid-state reaction. *Materials (Basel, Switzerland)* 16(22), 7170 (2023). <https://doi.org/10.3390/ma16227170>.
137. S.J. Park, H. Kwak, H.S. Kim, J. Bang, H. Park, O. Park, T.W. Kim, and S. Kim, Evolution of electrical transport properties in FeTe₂-CoTe₂ solid solution system for optimum thermoelectric performance. *J. Alloys Compd.* 960, 170850 (2023). <https://doi.org/10.1016/j.jallcom.2023.170850>.
138. J. Prado-Gonjal, E. García-Calvo, J. Gainza, O.J. Durá, C. Dejoie, N.M. Nemes, J.L. Martínez, J.A. Alonso, and F. Serrano-Sánchez, Optimizing thermoelectric properties through compositional engineering in Ag-deficient AgSbTe₂ synthesized by arc melting. *ACS Appl. Electron. Mater.* 6(5), 2969 (2024). <https://doi.org/10.1021/acsaelm.3c01653>.
139. A. Bhui, S. Das, R. Arora, U. Bhat, P. Dutta, T. Ghosh, R. Pathak, R. Datta, U.V. Waghmare, and K. Biswas, Hg doping induced reduction in structural disorder enhances the thermoelectric performance in AgSbTe₂. *J. Am. Chem. Soc.* 145(46), 25392 (2023). <https://doi.org/10.1021/jacs.3c09643>.
140. R. Rani and M.M. Sinha, Recent advances in two-dimensional transition metal oxides and Di-chalcogenides as efficient thermoelectric materials. *Phys. Scr.* (2024). <https://doi.org/10.1088/1402-4896/ad25cf>.
141. K. Rogdakis, N. Karakostas, and E. Kymakis, Up-scalable emerging energy conversion technologies enabled by 2D materials: from miniature power harvesters towards grid-connected energy systems. *Energy Environ. Sci.* 14(6), 3352 (2021). <https://doi.org/10.1039/D0EE04013D>.
142. M. Srivastava, S. Banerjee, S. Bairagi, P. Singh, B. Kumar, P. Singh, R.D. Kale, D.M. Mulvihill, and S.W. Ali, Recent progress in molybdenum disulfide (MoS₂) based flexible nanogenerators: an inclusive review. *Chem. Eng. J.* (2023). <https://doi.org/10.1016/j.cej.2023.147963>.
143. M.A.M. Hasan, Y. Wang, C.R. Bowen, and Y. Yang, 2D nanomaterials for effective energy scavenging. *Nano-Micro Lett.* 13, 1 (2021). <https://doi.org/10.1007/s40820-021-00603-9>.
144. Y. Jia, Q. Jiang, H. Sun, P. Liu, D. Hu, Y. Pei, W. Liu, X. Crispin, S. Fabiano, Y. Ma, and Y. Cao, Wearable thermoelectric materials and devices for self-powered electronic systems. *Adv. Mater.* 33(42), 2102990 (2021). <https://doi.org/10.1002/adma.202102990>.
145. M. Birkholz and R. Rudert, Interatomic distances in pyrite-structure disulfides: a case for ellipsoidal modeling of sulfur ions.

- Phys. Status. Sol. (B)* 245, 1858 (2008). <https://doi.org/10.1002/pssb.200879532>.
146. V. Kumar Gudelli, V. Kanchana, G. Vaitheeswaran, A. Svane, and N.E. Christensen, Thermoelectric properties of chalcopyrite type CuGaTe_2 and chalcocite CuSbS_2 . *J. Appl. Phys.* 114, 223707 (2013). <https://doi.org/10.1063/1.4842095>.
 147. R. Murphy and D.R. Strongin, Surface reactivity of pyrite and related sulfides. *Surf. Sci. Rep.* 64(1), 1 (2009). <https://doi.org/10.1016/j.surfrep.2008.09.002>.
 148. D. Zhang, C. Zhang, X. Li, and A. Qyyum, Layered iron pyrite for ultrafast photonics application. *Nanophotonics* 9, 2515 (2020).
 149. C. Uhlig, E. Guenes, A.S. Schulze, M.T. Elm, P.J. Klar, and S. Schlecht, Nanoscale FeS_2 (pyrite) as a sustainable thermoelectric material. *J. Electron. Mater.* 43, 2362 (2014). <https://doi.org/10.1007/s11664-014-3065-x>.
 150. L. Pauling, Covalent chemical bonding of transition metals in pyrite, cobaltite, skutterudite, millerite and related minerals. *Can. Miner.* 16, 447 (1978).
 151. Z.H. Ge, X. Liu, D. Feng, J. Lin, and J. He, High-performance thermoelectricity in nanostructured earth-abundant copper sulfides bulk materials. *Adv. Energy Mater.* 6(16), 1600607 (2016). <https://doi.org/10.1002/aenm.201600607>.
 152. M. Gholami, Z. Hajjahmadi, and S.S. Naghavi, Unlocking the potential of coinage-based quaternary chalcogenides for thermoelectricity. *J. Mater. Chem. A Mater.* 12, 5846 (2024). <https://doi.org/10.1039/D3TA07747K>.
 153. T. Parashchuk, O. Cherniushok, O. Smitiukh, O. Marchuk, and K.T. Wojciechowski, Structure evolution and bonding inhomogeneity toward high thermoelectric performance in $\text{Cu}_2\text{CoSnS}_{4-x}\text{Se}_x$ materials. *Chem. Mater.* 35(12), 4772 (2023). <https://doi.org/10.1021/acs.chemmater.3c00586>.
 154. M. Abubakar, Z. Abbas, A. Naz, H.W. Khalil, M.A. Khan, H. Kim, K. Khan, M. Ouladmane, S. Rehman, D.K. Kim, and M.F. Khan, First principles quantum analysis of structural, electronic, optical and thermoelectric properties of XCu_2GeQ_4 ($X = \text{Ba}$, Sr and $Q = \text{S}$, Se) for energy applications. *Opt. Quantum Electron.* 55(10), 849 (2023). <https://doi.org/10.1007/s11082-023-05136-6>.
 155. P. Gressier, A. Meerschaut, L. Guemas, J. Rouxel, and P. Monceau, New one-dimensional Vb transition metal tetrachalcogenides structural and transport properties. *J. Phys. Colloq.* 44, C3-1741 (1983). <https://doi.org/10.1051/jphyscol/1983104>.
 156. C.R. Roucaut Ayrolesf, P. Gressiert, and A. Meerschaut, Electron microscopy study of transition-metal tetrachalcogenide (MSe_4) n I ($M = \text{Nb}$, Ta). *J. Phys. C Solid State Phys.* 17, 2993 (1984). <https://doi.org/10.1088/0022-3719/17/17/007>.
 157. R.R. Chianelli and M.B. Dines, Reaction of N-butyllithium with trichalcogenides. *Inorg. Chem.* 14(10), 2417 (1975). <https://doi.org/10.1021/ic50152a023>.
 158. A. Patra and C.S. Rout, Anisotropic quasi-one-dimensional layered transition-metal trichalcogenides: synthesis, properties and applications. *RSC Adv.* 10, 36413 (2020). <https://doi.org/10.1039/D0RA07160A>.
 159. S.R. Yashas, H.P. Shivharaju, T. Thinley, K.S. Pushparaj, A. Maleki, and B. Shahmoradi, Facile synthesis of SnO_2 2D nanoflakes for ultrasound-assisted photodegradation of tetracycline hydrochloride. *Int. J. Environ. Sci. Technol.* 17, 2593 (2020). <https://doi.org/10.1007/s13762-020-02636-w>.
 160. B.J. Kooi and M. Wuttig, Chalcogenides by design: functionality through metavalent bonding and confinement. *Adv. Mater.* 32, 1908302 (2020). <https://doi.org/10.1002/adma.201908302>.
 161. Z. Lu, G.P. Neupane, G. Jia, H. Zhao, D. Qi, Y. Du, Y. Lu, and Z. Yin, 2D materials based on main group element compounds: phases, synthesis, characterization, and applications. *Adv. Funct. Mater.* 30(40), 2001127 (2020). <https://doi.org/10.1002/adfm.202001127>.
 162. J. Wang, P. Li, T. Cai, D.D. Yang, and W.W. Xiong, Four two-dimensional ternary selenides based on group 13 and 14 metals: syntheses, crystal structures, and electrochemical properties. *J. Solid State Chem.* 263, 88 (2018). <https://doi.org/10.1016/j.jssc.2018.04.018>.
 163. A. Shafique and Y.H. Shin, Thermoelectric and phonon transport properties of two-dimensional IV–VI compounds. *Sci. Rep.* 7, 506 (2017). <https://doi.org/10.1038/s41598-017-00598-7>.
 164. B. Mukherjee, Y. Cai, H.R. Tan, Y.P. Feng, E.S. Tok, and C.H. Sow, NIR Schottky photodetectors based on individual single-crystalline GeSe nanosheet. *ACS Appl. Mater. Interfaces* 5(19), 9594 (2013). <https://doi.org/10.1021/am402550s>.
 165. R. Fei, W. Kang, and L. Yang, Ferroelectricity and phase transitions in monolayer group-IV monochalcogenides. *Phys. Rev. Lett.* 117, 097601 (2016). <https://doi.org/10.1103/PhysRevLett.117.097601>.
 166. Y. Wei, J. He, Q. Zhang, C. Liu, A. Wang, H. Li, and T. Zhai, Synthesis and investigation of layered GeS as a promising large capacity anode with low voltage and high efficiency in full-cell Li-ion batteries. *Mater. Chem. Front.* 1, 1607 (2017). <https://doi.org/10.1039/C7QM00060J>.
 167. J.O. Morales-Ferreiro, D.E. Diaz-Droguett, D. Celentano, and T. Luo, First-principles calculations of thermoelectric properties of IV–VI chalcogenides 2D materials. *Front. Mech. Eng.* 3, 15 (2017). <https://doi.org/10.3389/fmech.2017.00015>.
 168. F. Li, X. Liu, Y. Wang, and Y. Li, Germanium monosulfide monolayer: a novel two-dimensional semiconductor with a high carrier mobility. *J. Mater. Chem. C* 4, 2155 (2016). <https://doi.org/10.1039/C6TC00454G>.
 169. Z.Y. Hu, K.Y. Li, Y. Lu, Y. Huang, and X.H. Shao, High thermoelectric performances of monolayer SnSe allotropes. *Nanoscale* 9, 16093 (2017).
 170. T.A. Wubieneh, C.L. Chen, P.C. Wei, S.Y. Chen, and Y.Y. Chen, The effects of Ge doping on the thermoelectric performance of P-type polycrystalline SnSe. *RSC Adv.* 6, 114825 (2016).
 171. G.K. Solanki, M.P. Deshpande, M.K. Agarwal, P.D. Patel, and S.N. Vaidya, Thermoelectric power factor measurements in GeSe single crystals grown using different transporting agents. *J. Mater. Sci. Lett.* 22, 985 (2003). <https://doi.org/10.1023/A:1024724922435>.
 172. J.M. Hodges, S. Hao, J.A. Grovogui, X. Zhang, T.P. Bailey, X. Li, Z. Gan, Y.-Y. Hu, C. Uher, V.P. Dravid, C. Wolverton, and M.G. Kanatzidis, Chemical insights into $\text{PbSe}-X\%\text{HgSe}$: high power factor and improved thermoelectric performance by alloying with discordant atoms. *J. Am. Chem. Soc.* 140(51), 18115 (2018). <https://doi.org/10.1021/jacs.8b11050>.
 173. H. Zhou, K. Cheng, X. Meng, J. Li, and W. Li, Layer-structured GaGeTe compound as a promising thermoelectric material. *ACS Appl. Energy Mater.* 6(8), 4264 (2023). <https://doi.org/10.1021/acsaem.3c00198>.
 174. A.K. Munirathnappa, H. Lee, and I. Chung, Recent advances in ultrahigh thermoelectric performance material SnSe. *Mater. Lab* 2(1), 220056 (2022). <https://doi.org/10.54227/mlab.20220056>.
 175. J. Wei, L. Yang, Z. Ma, P. Song, M. Zhang, J. Ma, F. Yang, and X. Wang, Review of current high-ZT thermoelectric materials. *J. Mater. Sci.* 55, 12642 (2020). <https://doi.org/10.1007/s10853-020-04949-0>.
 176. Z. Abbas, K. Fatima, S. Hussain, S. Al-Qaisi, A. Parveen, S. Muhammad, A.R. Chaudhry, A.G. Al-Sehemi, and M. Aslam, First-principles calculations of structural, electronic, optical and thermoelectric properties of doped binary chalcogenides $\text{Sn}_{1-x}\text{A}_x\text{Se}$ ($A = \text{Au}$ and Ag) for energy applications. *J. Solid State Chem.* 328, 124357 (2023). <https://doi.org/10.1016/j.jssc.2023.124357>.
 177. G.M. Mustafa, S. Saba, N.A. Noor, A. Laref, M.A. El-Rahman, Z. Farooq, R.B. Behram, and Z. Ullah, First-principles

- calculations to investigate $\text{HgY}_2\text{S}/\text{Se}_4$ spinel chalcogenides for optoelectronic and thermoelectric applications. *J. Market. Res.* 22, 97 (2023). <https://doi.org/10.1016/j.jmrt.2022.11.119>.
178. S. Li, Z. Li, J. Duan, S. Lou, and S. Zhou, Ag, Pb co-doped SnSe high performance thermoelectric materials. *J. Phys. D Appl. Phys.* (2024). <https://doi.org/10.1088/1361-6463/ad2d94>.
 179. L. Xu, X. Wang, Y. Wang, Z. Gao, X. Ding, and Y. Xiao, Enhanced average power factor and ZT value in PbSe thermoelectric material with dual interstitial doping. *Energy Environ. Sci.* 17(5), 2018 (2024). <https://doi.org/10.1039/D3EE04539K>.
 180. M. Zhang, Z. Gao, Q. Lou, Q. Zhu, J. Wang, Z. Han, C. Fu, and T. Zhu, Achieving high carrier mobility and thermal stability in plainified rhombohedral GeTe thermoelectric materials with ZT > 2. *Adv. Funct. Mater.* 34(6), 2307864 (2024). <https://doi.org/10.1002/adfm.202307864>.
 181. Z. Liu, Z. Guo, and L. Deng, Preparation of high-performance Mn-doped SnTe materials at high pressure and high temperature. *Inorg. Chem.* 63(12), 5389 (2024). <https://doi.org/10.1021/acs.inorgchem.3c03991>.
 182. C. Gayner and K.K. Kar, Recent advances in thermoelectric materials. *Prog. Mater. Sci.* 83, 330 (2016). <https://doi.org/10.1016/j.pmatsci.2016.07.002>.
 183. E.J. Menke, Q. Li, and R.M. Penner, Bismuth telluride (Bi_2Te_3) nanowires synthesized by cyclic electrodeposition/stripping coupled with step edge decoration. *Nano Lett.* 4, 2009 (2004).
 184. M. Martín-González, A.L. Prieto, R. Gronsky, T. Sands, and A.M. Stacy, High-density 40 Nm diameter Sb-rich $\text{Bi}_{2-x}\text{Sb}_x\text{Te}_3$ nanowire arrays. *Adv. Mater.* 15(12), 1003 (2003). <https://doi.org/10.1002/adma.200304781>.
 185. Z. Soleimani, S. Zoras, B. Ceranic, S. Shahzad, and Y. Cui, A review on recent developments of thermoelectric materials for room-temperature applications. *Sustain. Energy Technol. Assess.* 37, 100604 (2020). <https://doi.org/10.1016/j.seta.2019.100604>.
 186. M. Shtern, M. Rogachev, Y. Shtern, A. Sherchenkov, A. Babich, E. Korchagin, and D. Nikulin, Thermoelectric properties of efficient thermoelectric materials on the basis of bismuth and antimony chalcogenides for multisection thermoelements. *J. Alloys Compd.* 877, 160328 (2021). <https://doi.org/10.1016/j.jallcom.2021.160328>.
 187. A. Manabe, A. Mitsuishi, and H. Yoshinaga, Infrared lattice reflection spectra of II–VI compounds. *Jpn. J. Appl. Phys.* 6, 593 (1967). <https://doi.org/10.1143/JJAP.6.593>.
 188. M.K. Fuccillo, M.E. Charles, Y.S. Hor, S. Jia, and R.J. Cava, Low temperature thermoelectric properties of $\text{Bi}_{2-x}\text{Sb}_x\text{TeSe}_2$ crystals near the n-p crossover. *Solid State Commun.* 152(14), 1208 (2012). <https://doi.org/10.1016/j.ssc.2012.04.062>.
 189. G.S. Hegde and A.N. Prabhu, A review on doped/composite bismuth chalcogenide compounds for thermoelectric device applications: various synthesis techniques and challenges. *J. Electron. Mater.* 51, 2014 (2022).
 190. W. Liu, K.C. Lukas, K. McEnaney, S. Lee, Q. Zhang, C.P. Opeil, G. Chen, and Z. Ren, Studies on the Bi_2Te_3 - Bi_2Se_3 - Bi_2S_3 system for mid-temperature thermoelectric energy conversion. *Energy Environ. Sci.* 6, 552 (2013).
 191. S. Aminorroaya Yamini, R. Santos, R. Fortulan, A.A. Gazder, A. Malhotra, D. Vashae, I. Serhiienko, and T. Mori, Room-temperature thermoelectric performance of n-type multiphase pseudobinary Bi_2Te_3 - Bi_2S_3 compounds: synergic effects of phonon scattering and energy filtering. *ACS Appl. Mater. Interfaces* 15, 19220 (2023).
 192. H. Mamur, M.A. Üstüner, H. Korucu, and M.R.A. Bhuiyan, A review of the performance evaluation of thermoelectric nanostructure materials $\text{Bi}_{2-x}\text{Sb}_x\text{Te}_3$ ($0.20 \leq x \leq 1.80$). *Clean. Chem. Eng.* 6, 100101 (2023).
 193. F. Hao, P. Qiu, Y. Tang, S. Bai, T. Xing, H.-S. Chu, Q. Zhang, P. Lu, T. Zhang, D. Ren, J. Chen, X. Shi, and L. Chen, High efficiency Bi_2Te_3 -based materials and devices for thermoelectric power generation between 100 and 300 °C. *Energy Environ. Sci.* 9, 3120 (2016). <https://doi.org/10.1039/C6EE02017H>.
 194. H.S. Kim, N.A. Heinz, Z.M. Gibbs, Y. Tang, S.D. Kang, and G.J. Snyder, High thermoelectric performance in $(\text{Bi}_{0.25}\text{Sb}_{0.75})_2\text{Te}_3$ due to band convergence and improved by carrier concentration control. *Mater. Today* 20(8), 452 (2017). <https://doi.org/10.1016/j.mattod.2017.02.007>.
 195. T.J. Zhu, L.P. Hu, X.B. Zhao, and J. He, New insights into intrinsic point defects in V_2VI_3 thermoelectric materials. *Adv. Sci.* 3, 1600004 (2016). <https://doi.org/10.1002/advs.201600004>.
 196. Y. Pan, U. Aydemir, J.A. Grovogui, I.T. Witting, R. Hanus, Y. Xu, J. Wu, C.-F. Wu, F.-H. Sun, H.-L. Zhuang, J.-F. Dong, J.-F. Li, V.P. Dravid, and G.J. Snyder, Melt-centrifuged $(\text{Bi}, \text{Sb})_2\text{Te}_3$: engineering microstructure toward high thermoelectric efficiency. *Adv. Mater.* 30, 1802016 (2018). <https://doi.org/10.1002/adma.201802016>.
 197. Y. Luo, Y. Zheng, Z. Luo, S. Hao, C. Du, Q. Liang, Z. Li, K.A. Khor, K. Hippalgaonkar, J.W. Xu, Q. Yan, C. Wolverton, and M.G. Kanatzidis, n-Type SnSe_2 oriented-nanoplate-based pellets for high thermoelectric performance. *Adv. Energy Mater.* 8, 1702167 (2018). <https://doi.org/10.1002/aenm.201702167>.
 198. G.S. Hegde, A.N. Prabhu, R.Y. Huang, and Y.K. Kuo, Reduction in thermal conductivity and electrical resistivity of indium and tellurium co-doped bismuth selenide thermoelectric system. *J. Mater. Sci. Mater. Electron.* 31, 19511 (2020).
 199. G.S. Hegde, A.N. Prabhu, A. Rao, and M.K. Chattopadhyay, Enhancement in thermoelectric figure of merit of bismuth telluride system due to tin and selenium co-doping. *Mater. Sci. Semicond. Process.* 127, 105645 (2021). <https://doi.org/10.1016/j.mssp.2020.105645>.
 200. Q. Zhu, S. Wang, X. Wang, A. Suwardi, M.H. Chua, X.Y.D. Soo, and J. Xu, Bottom-up engineering strategies for high-performance thermoelectric materials. *Nano-Micro Lett.* 13(1), 119 (2021). <https://doi.org/10.1007/s40820-021-00637-z>.
 201. J. Mao, Z. Liu, and Z. Ren, Size effect in thermoelectric materials. *npj Quantum Mater.* 1, 16028 (2016). <https://doi.org/10.1038/npjquantmats.2016.28>.
 202. H.A. Chen, H. Sun, C.R. Wu, Y.X. Wang, P.H. Lee, C.W. Pao, and S.Y. Lin, Single-crystal antimonene films prepared by molecular beam epitaxy: selective growth and contact resistance reduction of the 2D material heterostructure. *ACS Appl. Mater. Interfaces* 10, 15058 (2018).
 203. M. Fortin-Deschênes, O. Waller, T.O. Menteş, A. Locatelli, S. Mukherjee, F. Genuzio, P.L. Levesque, A. Hébert, R. Martel, and O. Moutanabbir, Synthesis of antimonene on germanium. *Nano Lett.* 17, 4970 (2017).
 204. X. Wu, Y. Shao, H. Liu, Z. Feng, Y.-L. Wang, J.-T. Sun, C. Liu, J.-O. Wang, Z.-L. Liu, S.-Y. Zhu, Y.-Q. Wang, S.-X. Du, Y.-G. Shi, K. Ibrahim, and H.-J. Gao, Epitaxial growth and air-stability of monolayer antimonene on PdTe_2 . *Adv. Mater.* 29, 1605407 (2017). <https://doi.org/10.1002/adma.201605407>.
 205. G.S. Hegde, A.N. Prabhu, A. Rao, and P.D. Babu, Enhancement of thermoelectric performance of n-doped $\text{Bi}_2\text{Te}_{2.7}\text{Se}_{0.3}$ compounds. *Physica B* 584, 412087 (2020). <https://doi.org/10.1016/j.physb.2020.412087>.
 206. Q. Han, P.-A. Zong, H. Liu, Z. Zhang, K. Shen, M. Liu, Z. Mao, Q. Song, and S. Bai, Advancing thermoelectric performance of Bi_2Te_3 below 400 K. *ACS Appl. Mater. Interfaces* (2024). <https://doi.org/10.1021/acsami.4c03307>.
 207. R. Ren, P. Qin, J. Song, Y. Qin, W. Li, Y. Wang, X. Yang, J. Li, W. Löser, and C. Cao, Crystal growth and thermoelectric

- properties of Sn-doped Bi_2Se_3 . *J. Cryst. Growth* 627, 127510 (2024). <https://doi.org/10.1016/j.jcrysgro.2023.127510>.
208. T.Y. Zhong, Y. Wang, X. Yang, L. Yu, J. Feng, and Z.H. Ge, Ultralow thermal conductivity and enhanced thermoelectric properties realized in polycrystalline $\text{Bi}_2\text{S}_2\text{Se}$ via carrier and microstructure modulation. *ACS Appl. Energy Mater.* 7(8), 3424 (2024). <https://doi.org/10.1021/acsaem.4c00197>.
209. W. Yang, W. Le, J. Lyu, J. Li, Z. Chen, Q. Zhang, S. Liu, X. Li, and J. Shuai, Enhancing thermoelectric performance in P-type Sb_2Te_3 -based compounds through Nb-Ag co-doping with donor-like effect. *Small* 20(12), 2307798 (2024). <https://doi.org/10.1002/sml.202307798>.
210. S. Ruamruk, B. Chayasombat, K. Singsoog, and T. Seetawan, Thermoelectric properties of Sb_2Te_3 ink fabricated by screen-printing technique. *J. Electron. Mater.* (2024). <https://doi.org/10.1007/s11664-024-10996-z>.
211. X. Chen and R. Fan, Low-temperature hydrothermal synthesis of transition metal dichalcogenides. *Chem. Mater.* 13(3), 802 (2001). <https://doi.org/10.1021/cm000517+>.
212. X. Zhang, G. Ma, and J. Wang, Hydrothermal synthesis of two-dimensional MoS_2 and its applications. *Tungsten* 1, 59 (2019). <https://doi.org/10.1007/s42864-019-00014-9>.
213. U. Alli, S.J. Hettiarachchi, and S. Kellici, Chemical functionalisation of 2D materials by batch and continuous hydrothermal flow synthesis. *Chem. Eur. J.* 26, 6447 (2020). <https://doi.org/10.1002/chem.202000383>.
214. G. Tang, W. Wei, J. Zhang, Y. Li, X. Wang, G. Xu, C. Chang, Z. Wang, Y. Du, and L.D. Zhao, Realizing high figure of merit in phase-separated polycrystalline $\text{Sn}_{1-x}\text{Pb}_x\text{Se}$. *J. Am. Chem. Soc.* 138, 13647 (2016).
215. Y. Zheng, X.L. Shi, H. Yuan, S. Lu, X. Qu, W.D. Liu, L. Wang, K. Zheng, J. Zou, and Z.G. Chen, A synergy of strain loading and laser radiation in determining the high-performing electrical transports in the single Cu-doped SnSe microbelt. *Mater. Today Phys.* 13, 100198 (2020). <https://doi.org/10.1016/j.mtphys.2020.100198>.
216. Z. Zhou, W. Zhang, Y. Zheng, Y. Yang, B. Wei, C. Liu, J. Le Lan, C.W. Nan, and Y.H. Lin, Advances in N-type $\text{Bi}_2\text{O}_2\text{Se}$ thermoelectric materials: progress and perspective. *Mater. Today Phys.* 39, 101292 (2023). <https://doi.org/10.1016/j.mtphys.2023.101292>.
217. S.K. Kihoi, U.S. Shenoy, J.N. Kahi, H. Kim, D.K. Bhat, and H.S. Lee, Tailoring the thermoelectric performance of the layered topological insulator SnSb_2Te_4 through Bi positional doping at the Sn and Sb cation sites. *ACS Appl. Electron. Mater.* 5, 4504 (2023).

Publisher's Note Springer Nature remains neutral with regard to jurisdictional claims in published maps and institutional affiliations.